The Astrophysical Journal, 978:47 (17pp), 2025 January 01 https://doi.org/10.3847/1538-4357/ad944a

Once a Triple, Not Always a Triple: The Evolution of Hierarchical Triples That Yield Merged Inner Binaries

Cheyanne Shariat[1,2], Smadar Naoz[2,3], Kareem El-Badry[1], Antonio C. Rodriguez[1], Bradley M. S. Hansen[2,3], Isabel Angelo[2], and Alexander P. Stephan[4]
[1] Department of Astronomy, California Institute of Technology, 1200 East California Boulevard, Pasadena, CA 91125, USA; cshariat@caltech.edu
[2] Department of Physics and Astronomy, University of California, Los Angeles, CA 90095, USA
[3] Mani L. Bhaumik Institute for Theoretical Physics, University of California, Los Angeles, CA 90095, USA
[4] Department of Physics and Astronomy Vanderbilt University, Nashville, TN 37235, USA
Received 2024 July 8; revised 2024 October 30; accepted 2024 November 15; published 2024 December 24

Abstract

More than half of all main-sequence (MS) stars have one or more companions, and many of those with initial masses $<8\,M_{\odot}$ are born in hierarchical triples. These systems feature two stars in a close orbit (the inner binary) while a tertiary star orbits them on a wider orbit (the outer binary). In hierarchical triples, three-body dynamics combined with stellar evolution drives interactions and, in many cases, merges the inner binary entirely to create a renovated "post-merger binary" (PMB). By leveraging dynamical simulations and tracking binary interactions, we explore the outcomes of merged triples and investigate whether PMBs preserve signatures of their three-body history. Our findings indicate that in 26%–54% of wide double white dwarf (DWD) binaries ($s \gtrsim 100$ au), the more massive white dwarf (WD) is a merger product, implying that these DWD binaries were previously triples. Overall, we estimate that $44\% \pm 14\%$ of observed wide DWDs originated in triple star systems and thereby have rich dynamical histories. We also examine MS+MS and MS+red giant mergers manifesting as blue straggler stars (BSSs). These PMBs have orbital configurations and ages similar to most observed BSS binaries. While the triple +merger formation channel can explain the observed chemical abundances, moderate eccentricities, and companion masses in BSS binaries, it likely only accounts for ∼20%–25% of BSSs. Meanwhile, we predict that the majority of observed single BSSs formed as collisions in triples and harbor long-period (>10 yr) companions. Furthermore, both BSS binaries and DWDs exhibit signatures of WD birth kicks.

Unified Astronomy Thesaurus concepts: Stellar mergers (2157); Three-body problem (1695); Blue straggler stars (168); White dwarf stars (1799)

1. Introduction

Observational and theoretical studies clearly show that most main-sequence (MS) stars form and evolve with one or more stellar companion (e.g., D. Raghavan et al. 2010; A. Tokovinin 2014a; M. Moe & R. Di Stefano 2017; S. S. R. Offner et al. 2023, see latter for a review). For multiple star systems, there are numerous possible processes that govern the early stages of formation. Fragmentation models suggest that most multiple star systems form via the gravitational collapse of overdense regions that arise in cores, filaments, or massive accretion disks (e.g., R. B. Larson 1972; F. C. Adams et al. 1989; S.-I. Inutsuka & S. M. Miyama 1992; A. A. Goodman et al. 1993; K. M. Kratter et al. 2008; M. R. Krumholz et al. 2009; D. M.-A. Meyer et al. 2018). Dynamical capture, evolution, and migration models supply even more channels for the formation of multiple systems (e.g., E. C. Ostriker 1994; M. R. Bate & I. A. Bonnell 1997; E. C. Ostriker et al. 1999; J. E. Tohline 2002; N. Moeckel & J. Bally 2007; M. R. Bate 2012; A. T. Lee et al. 2019; C. Cournoyer-Cloutier et al. 2021).

Naturally, and from stability arguments, the protostars that form in these regions tend toward hierarchical configurations (G. Duchêne & A. Kraus 2013). In triple systems, for example, hierarchy manifests with two stars residing in a close orbit (the inner binary) while a tertiary star orbits around them on a wider orbit (the outer binary). In dense open and globular clusters, where dynamical interactions are more frequent, hierarchical triples are commonplace and help shape the stellar population (e.g., D. W. Latham 2007; A. M. Geller et al. 2009; N. Leigh & A. Sills 2011; A. M. Geller & R. D. Mathieu 2012; A. P. Milone et al. 2012; A. M. Geller et al. 2013; N. W. C. Leigh & A. M. Geller 2013). Stellar triples are also abundant in the galactic field (e.g., D. Raghavan et al. 2010; A. Tokovinin 2014a). For example, 40% of short-period binaries with 0.5–$1.5\,M_{\odot}$ companions have an additional companion (A. A. Tokovinin 1997; A. Tokovinin 2014a). Among contact binaries, a similar 42% are part of triples (T. Pribulla & S. M. Rucinski 2006). Further studies have demonstrated the abundance of triple systems by observed eclipsing binaries (S. Rappaport et al. 2013; K. E. Conroy et al. 2014) and stellar multiplicity studies (A. A. Tokovinin 1997; P. P. Eggleton et al. 2007; M. Moe & R. Di Stefano 2017). Recently, C. Shariat et al. (2023) performed a detailed investigation on the evolution of solar-type stars in hierarchical triples from their birth to their fate as white dwarfs (WDs). By comparing their dynamical simulations and Gaia observations, they predicted that 30%–40% of solar-type stars in the galactic neighborhood were formed in hierarchical triples.

During the evolution of hierarchical triples, the distant tertiary star will exchange angular momentum with the inner binary in a secular fashion, causing eccentricity-inclination oscillations: a process known as the eccentric Kozai–Lidov (EKL) mechanism (H. von Zeipel 1910; Y. Kozai 1962; M. L. Lidov 1962; S. Naoz 2016, see the latter for a review).

Large eccentricities induced in the inner binary from EKL cycles lead triples to interact (i.e., transfer mass) far more often than they would as isolated binaries (e.g., S. Naoz & D. C. Fabrycky 2014; A. P. Stephan et al. 2016; S. J. Cheng et al. 2019; S. Toonen et al. 2020; C. Shariat et al. 2023).[5] This makes triples an especially interesting channel to study binary exotica such as blue straggler stars (BSSs; A. M. Geller et al. 2013), cataclysmic variables (CVs; G. Nelemans et al. 2001; C. Knigge et al. 2011; A. F. Pala et al. 2017; C. Knigge et al. 2022), and post-common envelope binaries (e.g., S. Toonen & G. Nelemans 2013; M. Zorotovic et al. 2014; M. S. Hernandez et al. 2022; N. Yamaguchi et al. 2024a).

Beyond just mass transfer, interactions in the inner binary catalyzed by a distant companion can cause the inner binary to merge entirely (e.g., F. Antonini et al. 2017; E. Grishin & H. B. Perets 2022; H. P. Preece et al. 2022; A. A. Trani et al. 2022; A. S. Rajamuthukumar et al. 2023; C. Shariat et al. 2023; A. Dorozsmai et al. 2024). In such cases, the triple will become a binary where one star is a merger remnant and the other is the tertiary from the previous triple. We refer to these triples-turned-binaries as post-merger binaries (PMBs).

In this study, we explore the signatures of the evolution of PMBs from their triple birth to their binary fate. We investigate whether PMBs contain observable signatures that allude to their triple origin. For instance, the remnant star can be bluer and brighter than the main-sequence turnoff (e.g., A. R. Sandage 1953), have unusual chemical abundances (e.g., T. T. Hansen et al. 2016), have rapid or inclined rotation (e.g., A. Qureshi et al. 2018; E. Leiner et al. 2019; A. P. Stephan et al. 2020; S. Toonen et al. 2022), or contain two components with apparently discrepant ages (i.e., a non-coeval binary; T. M. Heintz et al. 2022).

We organize our study of triples-turned-binaries as follows. In Section 2, we outline the simulations that were used to evolve the triples and binaries for megayear to gigayear timescales. We then explore the three-body merger channel to form apparently discrepant wide double white dwarfs (DWDs; Section 3) and BSS binaries (Section 4). In Section 5, we examine the orbital configurations of triples with merged WD+MS or WD+RG inner binaries. In Section 6, we discuss other interesting outcomes of triples with mergers and their applications to observable stellar systems. Finally, in Section 7, we summarize our main results and conclusions.

2. Methodology

2.1. Physical Processes and Numerical Setup

C. Shariat et al. (2023) simulated ∼4000 hierarchical triple systems and dynamically evolved all three stars for over 10 Gyr. Following their setup, we consider a hierarchical triple system of masses m_1, m_2, on a tight inner orbit, and m_3 on a wider orbit about the inner binary. The three stars have radii R_1, R_2, and R_3. The orbital parameters include the inner (outer) semimajor axis a_1 (a_2), eccentricity e_1 (e_2), and inclination with respect to the total angular momentum i_1 (i_2). In C. Shariat et al. (2023), a robust sample ($\gtrsim$50%) of the three-body simulations that assumed a Kroupa initial mass function (IMF; P. Kroupa et al. 1993) resulted in a merged inner binary, turning the triple in a binary. In this study, we focus on the subset of these systems that lived on as PMBs.

In the simulations, C. Shariat et al. (2023) solved the equations of motion for the hierarchical triple up to the octupole level of approximation (see S. Naoz 2016, for the full set of equations). They also include general relativistic precession up to the first post-Newtonian order for the inner and outer orbit (e.g., S. Naoz et al. 2013). These precession approximations are sufficient to describe the dynamics within the mass ratios and scales studied here (e.g., S. Naoz et al. 2013; H. Lim & C. L. Rodriguez 2020; A. Kuntz 2022). Equilibrium tides are adopted for both inner binary members, following P. Hut (1980), P. P. Eggleton et al. (1998), and L. G. Kiseleva et al. (1998). This model includes rotational precession, tidal precession, and tidal dissipation (S. Naoz & D. C. Fabrycky 2014). For stars on the giant branch, the code switches to radiative tides following (A. P. Stephan et al. 2018; S. C. Rose et al. 2019).

Stellar evolution plays a crucial role in the evolution of triples (e.g., S. Naoz 2016; S. Naoz et al. 2016; S. Toonen et al. 2016, 2020, 2022; S. J. Cheng et al. 2019; A. S. Hamers et al. 2022; J. Stegmann et al. 2022; F. Kummer et al. 2023; C. Shariat et al. 2023). For example, the mass loss associated with the asymptotic giant branch (AGB) phase can re-trigger the EKL mechanism (H. B. Perets & K. M. Kratter 2012; B. J. Shappee & T. A. Thompson 2013; E. Michaely & H. B. Perets 2014; S. Naoz et al. 2016; A. P. Stephan et al. 2016, 2017). We thus follow the post-main-sequence evolution of stars using the Single Stellar Evolution (SSE) code (J. R. Hurley et al. 2000). See S. Naoz (2016), S. Naoz et al. (2016), A. P. Stephan et al. (2016, 2017, 2018, 2019, 2021), and I. Angelo et al. (2022) for a detailed description of the triple with stellar evolution code. If the inner binary experiences mass transfer or becomes tidally locked, the evolution of the inner binary is carried out using COSMIC (K. Breivik et al. 2020b), a suite for the Binary Stellar Evolution (BSE) code (J. R. Hurley et al. 2002) with additional modifications. We outline our general procedure for transferring between the three-body code and COSMIC in Section 2.2. In that Section, we also give an example evolution of a triple system that merged. For a more descriptive outline of implementing COSMIC, refer to C. Shariat et al. (2023).

The three-body simulations from C. Shariat et al. (2023) included two different models with slightly different initial ansatzes. Both models use a Kroupa IMF (P. Kroupa et al. 1993) from 1–8 $M_\odot$, but use different methods of sampling the initial inner and outer orbital periods. The first model chooses the inner and outer orbital periods independently from a log-normal period distribution with a mean of $\log(4.8/d)$ and a standard deviation of $\log(2.3/d)$ (A. Duquennoy & M. Mayor 1991). Then, the larger value is taken to the period of the outer orbit, and the smaller is taken as the period of the inner orbit. As the last step, we keep only systems that pass the hierarchy and stability criterion. Hierarchy is determined by the inequality (S. Naoz 2016):

$$\epsilon = \frac{a_1}{a_2}\frac{e_2}{1-e_2^2} < 0.1. \quad (1)$$

The stability criterion we use is (R. A. Mardling & S. J. Aarseth 2001):

$$\frac{a_2}{a_1} > 2.8\left(1+\frac{m_3}{m_1+m_2}\right)^{\frac{2}{5}}\frac{(1+e_2)^{\frac{2}{5}}}{(1-e_2)^{\frac{6}{5}}}\left(1-\frac{0.3i}{180^\circ}\right). \quad (2)$$

[5] Other hierarchical perturbations, such as flyby stars, can also excite high eccentricities in wide systems, leading to interactions (e.g., N. A. Kaib & S. N. Raymond 2014; E. Michaely & H. B. Perets 2016, 2019, 2020; E. Michaely 2021).

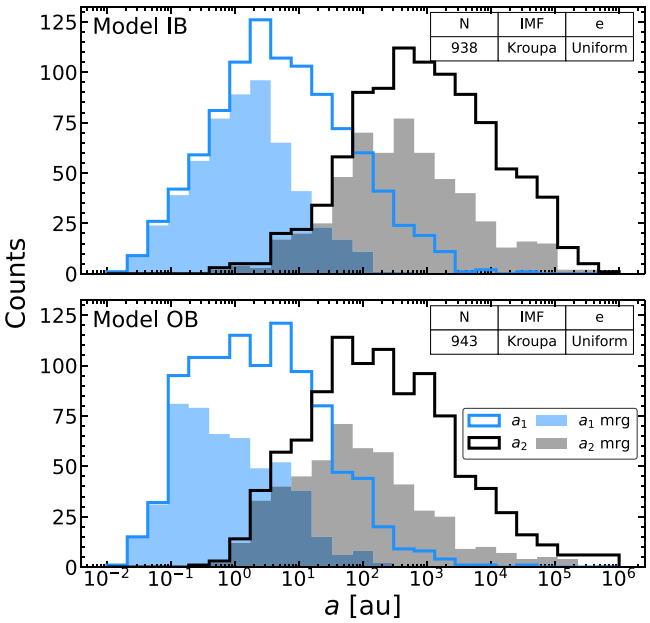

Figure 1. Initial conditions of the triple-star models. The solid line represents semimajor axes of all triples, while the shaded regions shows them for triples that experienced a merged inner binary during the three-body evolution. Both the inner and outer semimajor axes distributions were sampled from A. Duquennoy & M. Mayor (1991), but the bottom panel had a_2 sampled from A. Duquennoy & M. Mayor (1991). For that fixed value of a_2, a_1 was sampled until a stable combination was formed. In the top panel, both a_1 and a_2 were sampled independently from the distribution (see Section 2). In Model IB, 59% ($N = 553$) of all of the triples experienced a merged inner binary, and in Model OB, this fraction was 54% ($N = 509$; C. Shariat et al. 2023). In the inset tables, we show the total number of initial triples, their IMF, and initial eccentricities. The initial inclinations were chose to be isotropic for all triples.

We label this set of runs as "IB" (independent binary) following C. Shariat et al. (2023) because both the inner and outer period distributions are resampled independently. Therefore, this model effectively tests formation models where the inner and outer periods have no correlation. This could reflect independent fragmentation models and dynamical capture models (e.g., E. C. Ostriker 1994; D. M.-A. Meyer et al. 2018).

C. Shariat et al. (2023) also devised a second channel for sampling the orbital periods from the A. Duquennoy & M. Mayor (1991) distribution. In this model, they sampled the period of the outer orbit from the A. Duquennoy & M. Mayor (1991) distribution, and for that chosen orbit, resampled the period of the inner binary until a stable system was formed. If the sampled outer period was too small to physically allow for a stable inner orbit, we resampled the outer orbit. In this second channel for generating initial periods, a hierarchy of formation is assumed: the outer orbit formed first and limited the allowed (stable) configurations of the inner orbit. We label this set of runs as "OB" (outer binary) to denote that the OB has governance. Overall, the different sampling methods mean that triples in the OB model have closer inner binaries more often (Figure 1).

The initial semimajor axis distribution for Model IB is displayed in the top panel of Figure 1. We also show the initial a_1 (blue) and a_2 (black) distribution for the triples that led to a merged inner binary. The a_1 and a_2 distributions for Model IB closely resemble two Gaussians, whereas in the Model OB a_2 distribution is effectively Gaussian, while the a_1 distribution is a left-biased Gaussian constrained by the a_2 value. Overall, most inner binaries with close initial separations ($a_1 \lesssim 10$ au) experienced a merger. Furthermore, the inner binaries with closer tertiaries, which would induce stronger EKL effects, were more likely to merge. In Figure 1, we also show the total number of triples (N) for each model at $t = 0$, the IMF information, and the eccentricity distribution (assumed uniform for both). The initial inner and outer inclinations are chosen from an isotropic distribution.

In the IB Model, 59% ($N = 553$) of all of the triples experienced a merged inner binary, and in the OB model, this fraction is 54% ($N = 509$; C. Shariat et al. 2023). Across both models, 65 had destroyed inner binaries (i.e., no remnant star) and another 119 triples were unbound or disrupted by the merger event. Also, 19 PMBs were unable to be modeled in `COSMIC` beyond their merger age. This leaves behind 395 (415) survived PMBs in the IB (OB) model. The inner binaries that merged to produce PMBs are diverse, including mergers between MS, red giant (RG), and WD stars.

In Table 1, we show the abundance of the different outcomes from each model, including the various types of binary mergers. In this Table, we include the number of total completed triple simulations ("N Total") along with the number of those that had merged inner binaries ("N Merged Total"). "N Formed PMB" refers to the number of triples that had merged inner binaries and survived as PMBs. "N Disrupted" counts the times when the inner binary merger disrupted the triple. This includes cases where the merger did not leave behind a surviving star and cases where the merger event unbound the tertiary from the system. "N Double Merger" is the number of times where the inner binary and post-merger outer binary merged (discussed in Section 6.1). In the last six columns, we show the distribution for the different types of mergers among only the merged triples that survive as bound PMBs. The OB model had closer initial inner and outer binary separations, which led to a greater fraction of early MSMS mergers and double mergers. On the other hand, the IB model had a greater fraction of mergers that occurred later in the triple evolution, leading to more mergers involving RG and WD stars.

For both the IB and OB models, we also calculate the effect that kicks during WD formation would have on the orbits. Different sources have found support for WD kicks, and we briefly outline some here. Based on observations of the globular clusters and Monte Carlo modeling, WD kicks of a few kilometers per second prolong the core contraction of clusters, and this resolves the discrepancy between theory and observations (J. M. Fregeau et al. 2009). Moreover, WD birth kicks of $\sim$0.75 km s^{-1} resolve the discrepancy between binary population synthesis models and the observed separation distribution of WD binaries from Gaia (K. El-Badry & H.-W. Rix 2018). C. Shariat et al. (2023) also found that accounting for an agnostic $\sim$0.75 km s^{-1} kick was essential to reproducing the observed separation distribution of WD triples. More recently, measurements of WDMS binaries with current separations of a few astronomical unit show that most binaries have eccentricities above $\sim$0.15 and up to 0.8 (S. Shahaf et al. 2024). The separation of these systems suggests that they underwent mass transfer, though they are likely too distant to have experienced a common-envelope phase (e.g., F. Lagos et al. 2022; N. Yamaguchi et al. 2024b). Nevertheless, during mass transfer, the binaries should have presumably circularized through tides. WD kicks are one proposed mechanism to explain such binaries, though other mechanisms have not been ruled out (see S. Shahaf et al. 2024, and references therein).

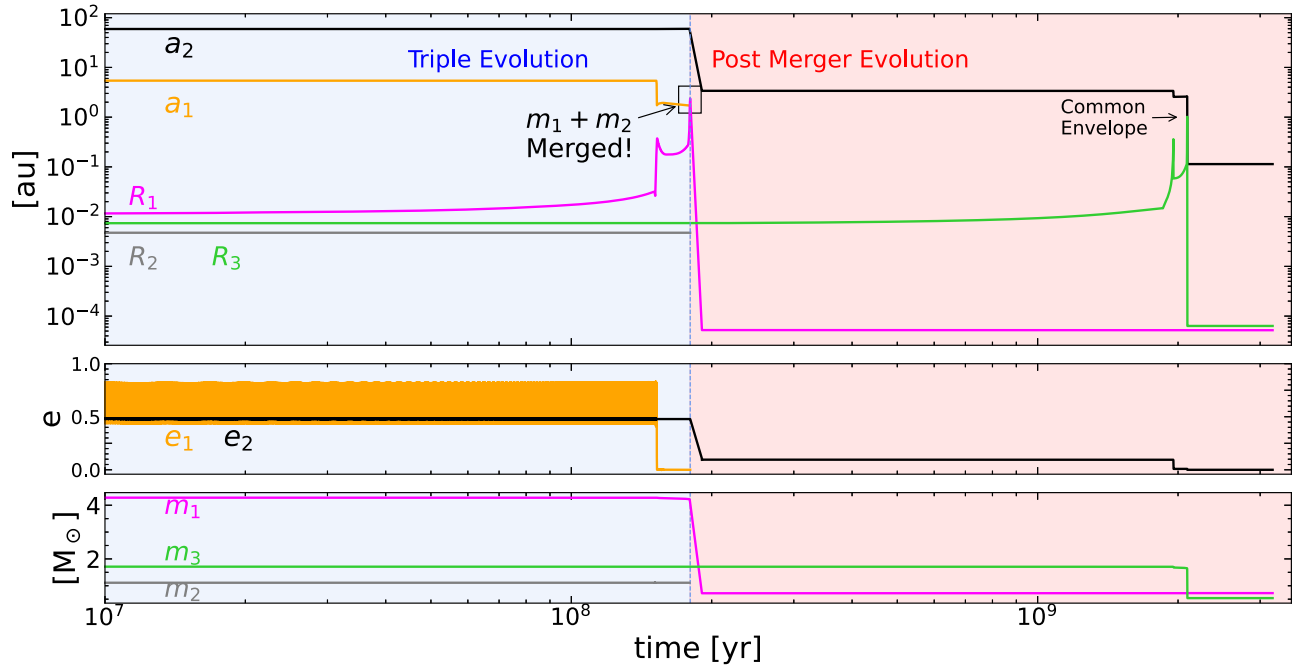

Figure 2. Example evolution of a triple that experienced a merged inner binary and became a post-merger binary (PMB). In the top panel, we track the evolution of the inner and outer semimajor axes (a_1 and a_2) and the radii for all three stars in the triple (R_1, R_2, and R_3). In the middle panel, we track the eccentricity of the inner (e_1) and outer (e_2) orbits. In the bottom panel, we show the evolution of the mass for all three stars (m_1, m_2, and m_3). The blue shaded region (labeled "Triple Evolution") is when the system was still a triple, and the red (labeled "Post Merger Evolution") shows its evolution as a binary after the two inner stars merged at $t \sim 189$ Myr. Initially, $m_1 = 4.3\ M_\odot$, $m_2 = 1.1\ M_\odot$, $m_3 = 1.7\ M_\odot$, $a_1 = 5.4$ au, $a_2 = 59.2$ au, $e_1 = 0.45$, and $e_2 = 0.47$. The more-massive m_1 evolves first onto the red giant branch (RGB) and then the asymptotic giant branch (AGB). During this time, it begins contact with m_2, which strips most of its envelope. Quickly, m_2 spirals into m_1 and leaves behind a C/O white dwarf with $0.72\ M_\odot$. This white dwarf is now in a binary orbit with the tertiary $m_3 = 1.7\ M_\odot$ In the "Post Merger Evolution" (red) region, the binary evolves steadily until m_3 starts moving off the main sequence and expands at $t = 1.35$ Gyr. Here, it undergoes common envelope evolution with the primary WD at 1.52 Gyr, at which point the orbit has shrunk significantly, and m_3 becomes a C/O WD. The end result is a double WD system in a 12 day period.

Table 1
Inner Binary Mergers

	N Triples	N Merged Total	N Formed PMB	N Disrupted	N Double Merger	Merger Type					
						MSMS	RGMS	RGRG	WDMS	WDRG	WDWD
Model IB	938	540	415	125	9	79	175	8	68	34	50
Model OB	943	473	395	78	27	106	133	13	92	24	27

Considering the strong possibility of WD kicks, we add the new models that assume an agnostic and modest kick during WD formation for all systems of the IB and OB models. The minor kick changes the eccentricity and semimajor axis of the outer orbit, generally by pumping the eccentricity and widening the orbit; we follow C. X. Lu & S. Naoz (2019) to calculate the new orbital parameters. For the complete protocol of applying a WD kick to the three-body evolution, refer to C. Shariat et al. (2023).

2.2. Evolving Beyond Merger

Of the entire sample of triple-star systems from C. Shariat et al. (2023), ∼50% had an inner binary that merged. These represented the systems where the inner binary (1) began to interact in the triple code and (2) after being put into COSMIC, were found to coalesce into one star. We put the binary into COSMIC to follow the moments leading up to the inner binary merging. In most cases, the merger leaves behind one star, creating a newly formed binary with the tertiary from the triple (m_3).

During the time that the inner binary was undergoing its interaction, we also followed the evolution of m_3 on these short timescales (often ∼Myr) to track any changes in mass or radius. If there were any changes to the tertiary that would change the orbital configuration during this time, they are applied. We calculate the new semimajor axis and eccentricity of the PMB based on (1) the previous triple's orbital parameters and (2) how long the inner binary interacted. If the interaction of the inner binary was larger than the outer orbital period (between the inner binary and the tertiary), then we assumed an adiabatic mass loss, and therefore, the eccentricity remained the same, and the semimajor axis expanded accordingly. If the mass loss occurred on times smaller than the orbital period, we applied a "kick" prescription to model the mass loss as being effectively instantaneous. In this case, the new eccentricity and semimajor axis were calculated following C. X. Lu & S. Naoz (2019). For more details on our procedure to calculate the orbital parameters of the PMB, see C. Shariat et al. (2023).

Now that the triple has become a PMB and its orbital configuration is identified, we again put the newly formed PMB into COSMIC and evolve until completion (often a few gigayears for most of the following analysis). In many cases, the triple and binary evolution is highly involved and leads to an interesting array of final binaries that were previously triples. We outline one example evolution in Figure 2. We

caution that both at this stage and in the interacting inner binary stage, COSMIC sets the eccentricity to zero. Thus, in all of our predictions, we underestimate the eccentricity of the short-period binaries, including PMBs.

2.2.1. Example Evolution of a Post-merger Binary

In Figure 2, we present an example of the evolution of a stellar triple that has $m_1 = 4.3\ M_\odot$, $m_2 = 1.1\ M_\odot$, $m_3 = 1.7\ M_\odot$, $a_1 = 5.4$ au, $a_2 = 59.2$ au, $e_1 = 0.45$, and $e_2 = 0.47$. The tertiary here excites only moderate eccentricity excitation (middle panel). After ∼189 Myr, the more-massive star (m_1) in the inner binary transitions from core helium burning and approaches the first AGB. Here, it inflates into Roche crossing, where it shrinks and circularizes the inner orbit and begins a sequence of events where the binary goes in and out of contact evolution. In the 1 Myr before the stars merged entirely, m_2 strips most of m_1's envelope during the first common envelope evolution, which removes $\sim 3\ M_\odot$ from the binary and leaves m_1 as a $0.93\ M_\odot$ naked helium star in the Hertzsprung Gap. During the final moments of the binary's life, m_2 spirals into m_1, expelling $\sim 1 M_\odot$ of mass and pushing the remnant star to the AGB. After this merger event settles, the new primary survives as an inflated AGB star (the result of $m_1 + m_2$ merging) and has an MS companion (m_3 from the triple). Tides from the inflated AGB star quickly shrink and circularize the new binary's orbit to $a = 3.4$ au. However, the enriched AGB star quickly has its mass ejected and forms a $0.72\ M_\odot$ WD at $t = 190$ Myr.

We are left with a new binary where the primary is a $0.72\ M_\odot$ WD and the tertiary is $m_3 = 1.7\ M_\odot$ MS star. Now, entering the "Post Merger" (red) region of the plot, simulated with COSMIC, the binary evolves steadily until m_3 starts to move off the MS. As m_3 expands at $t = 1.35$ Gyr, it undergoes common envelope evolution with the merged product, now the primary WD. The mass ejection persists until 1.52 Gyr, at which point the orbit has shrunk significantly, and m_3 is now a C/O WD, making a double WD system with a period of 12 days. This stage utilizes COSMIC, which assumes efficient tides and thus sets the eccentricity to zero.

The remaining binary is an example of a PMB that ended its eventful life as a circular DWD binary with an orbital period of 12 days, a primary mass of $0.72\ M_\odot$, and a secondary mass of $0.55\ M_\odot$. Throughout the evolution, the system could have been observed as a (1) BS binary system during the RGMS merger (e.g., E. Leiner et al. 2019), (2) cataclysmic variable-like binary during the second mass transfer episode, and (3) DWD with anomalous cooling ages, as observed in T. M. Heintz et al. (2022). Note that for ∼800 Myr during the post-merger evolution, the system was a WD+MS binary separated by a few astronomical unit. Observed ∼1 au WD +MS binaries have a deficit of massive WD components ($\gtrsim 0.8\ M_\odot$), which may hint at a lack of merger products (N. Hallakoun et al. 2023). We also find that the shortest WDMS binary in which the WD is a result of a previous WD+WD merger is ∼10 au, supporting that close WDMS systems are unlikely to have undergone a previous merger.

3. Double White Dwarfs

3.1. Observations of Double White Dwarfs

Stars with initial masses less than ~ 8–$10 M_\odot$ become white dwarfs. As a result, WDs are extremely common and represent the endpoint for 97% of stars in the Galaxy (G. Fontaine et al. 2001). After isolated single stars become white dwarfs, they no longer undergo nuclear fusion and, therefore, strictly cool over time. The cooling age of a WD is a function of its birth mass, with higher initial masses leading to longer cooling times and lower initial masses leading to shorter cooling times for single WDs. Therefore, accurate cooling models (e.g., P. Bergeron et al. 1995) allow single WDs to serve as precise age indicators.

T. M. Heintz et al. (2022) studied the ages of WDs in wide DWD binaries from the Gaia Early Data Release 3. The age of WDs in this sample was determined using a Monte Carlo SED-fitting approach from broadband photometry. Recently, T. M. Heintz et al. (2024) did a follow-up study where they re-derived the age estimated from spectroscopic data and found consistent values with the photometric evidence. Interestingly, they identified 283 DWDs with anomalous age measurements, representing 21%–36% of their sample. In these DWDs, the more-massive WD possesses a shorter cooling age than its less-massive companion with over 3σ confidence. This discrepancy was observed with both photometric and spectroscopic age estimates (T. M. Heintz et al. 2022, 2024), and it suggests that the less-massive WD was born from a more-massive main-sequence progenitor. This observation is not consistent with a monotonically increasing initial–final mass relation (IFMR), which leads to new interpretations.

One potential explanation for these peculiar observations is that the more-massive WD in the binary is the product of a prior merger event, suggesting that the DWD system was originally a triple. One example of a WD being formed from two merging stars is shown in the m_1+m_2 merger in Figure 2 and described in Section 2.2.1—here, an MS star merged with an AGB star, forming an already-evolved C/O WD. This merger remnant WD would presumably have a shorter cooling age than would be estimated from the isolated stellar evolution model for a WD of its mass.

C. Shariat et al. (2023) found that upward of 30% of stars in the solar neighborhood were born as triples, with over half of them experiencing a merger. This proposes a formation channel for the 21%–36% of DWDs that may potentially have merger remnants (T. M. Heintz et al. 2022). A 20% merger fraction is also consistent with binary population synthesis models (K. D. Temmink et al. 2020) and the multiplicity rate of WD progenitor stars (M. Moe & R. Di Stefano 2017), making the potential for a prior merger a great possibility.

Furthermore, N. Hallakoun et al. (2023) recently discovered an order-of-magnitude deficit of massive WD companions in ∼1 au binaries with F/M-dwarfs. At such separations, the binaries were likely to have undergone a phase of stable mass transfer and are unlikely to harbor a merger remnant because the stars are close. Since the massive WDs ($>0.8\ M_\odot$) are missing in this sample, a significant fraction of massive WDs in the field may be merger products (K. D. Temmink et al. 2020; N. Hallakoun et al. 2023). Given the likelihood that a fraction of field WDs are the result of previous mergers, we investigate whether the three-body formation channel can dynamically support a high merger rate of WDs in the galactic field (see Section 3.2).

3.2. Comparing Observed Double White Dwarfs to Theoretical Simulations

3.2.1. Cooling Ages and Masses

To calculate the total age of an observed WD, T. M. Heintz et al. (2022) summed the best-fit progenitor age (its MS

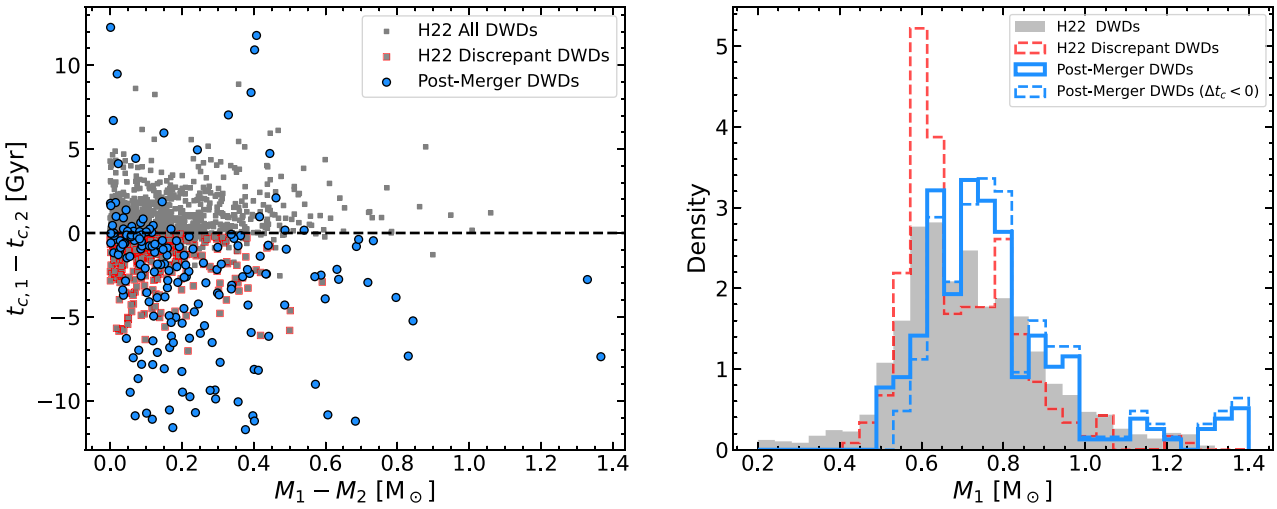

Figure 3. The cooling ages and mass of post-merged binaries that became DWDs ("Post-Merger DWDs") compared to observed DWDs with apparently discrepant ages from T. M. Heintz et al. (2022). Left panel: the difference in the cooling age between the more-massive DWD (subscript "1") and the less-massive WD (subscript "2") compared to their difference in mass. In gray, we show the observed systems, where those with a red outline are the discrepant DWDs. In blue, we show our simulated systems that experienced a merger and were DWDs at $t = 13.7$ Gyr. Right panel: the normalized distribution of the primary WD mass in observed wide DWDs (gray), observed discrepant DWDs (red dashed), the simulated post-merger DWDs (blue), and the simulated discrepant post-merger DWDs (blue dashed). The histograms are normalized such that the integrated area under the curve is 1.

lifetime) and the best-fit WD age based on its cooling track. To calculate the best-fit progenitor age, they mapped the current mass of the WD to a progenitor's zero-age main-sequence (ZAMS) mass using a shifted MESA IFMR (C. E. Fields et al. 2016). From the ZAMS mass, one can then calculate the total MS lifetime, assuming single stellar evolution. If there were a merger during the star's evolution, this age calculation method would give the wrong answer, leading to a discrepancy among the ages of stars in the binary DWDs. Since the study focuses on wide systems ($s \gtrsim 100$ au; T. M. Heintz et al. 2022), the probability of previous mass transfer between the two stars is unlikely, making the merger channel a potentially robust explanation for the observed discrepancies. Here, we seek to understand whether the PMBs that became DWDs in our theoretical simulations also possess similarly discrepant cooling ages and therefore, support the merger channel.

In Figure 3, we plot the cooling ages and masses of all of our post-merger DWDs after they evolved for 13.7 Gyr (blue). The total time of evolution does affect the difference in WD cooling ages, though it does govern how large the magnitude of the difference can be. We chose a conservative value that is likely higher than the true age of observed systems, which leads to larger cooling age differences in our simulations (though most of our DWDs formed in 1–10 Gyr). In both plots, we also show the values for the observed DWDs (gray) and the discrepant subset of observed DWDs (red outline). The masses and MS/WD lifetimes of the stars were calculated using `COSMIC`. Note that the oldest and coolest WDs would be too faint to be observed with Gaia, and therefore are missing in this sample.

Similar to Figure 7 in T. M. Heintz et al. (2022), the left panel of Figure 3 shows the cooling age difference as a function of the mass difference between the more-massive and less-massive WDs (subscript "1" and "2," respectively). Of the 163 post-merger DWDs in our sample, 80% exhibit discrepant cooling ages. In these systems, the merger history of the primary WD made the cooling age smaller than its less-massive companion. To check with uncertainties, we take the median cooling age uncertainty from the systems in T. M. Heintz et al. (2022) and find that it does not change the results. T. M. Heintz et al. (2022) found that 21%–43% of all wide DWDs exhibit such discrepancies in their cooling ages. Based on our simulated results, we can assume that this only accounts for 80% of the observed post-merger DWDs. Based on the aforementioned consistency, we attribute the anomalous ages of most observed systems to be a sign that their primary WD is a merger product. This would suggest that about 26%–54% of wide DWDs contain merger products. The presence of a merged WD today suggests that all of these systems were previously triples, like hierarchical triples. In this case, their three-body history provides more dynamical freedom compared to isolated binary evolution, which can explain their high frequency of mergers in the prior inner binary (e.g., S. Toonen et al. 2020; C. Shariat et al. 2023). A triple fraction of $40\% \pm 14\%$ is consistent with C. Shariat et al. (2023), who predicted that $\gtrsim$30% of solar-type stars were born in triples.

The right plot of Figure 3 shows the distribution of the primary WD mass in the DWD, normalized so that the area under the curve is unity. We display all observed DWDs in gray, the discrepant ones in red, the simulated post-merger DWDs in blue, and the discrepant simulated DWDs in dashed blue. Compared to all DWDs, the simulated post-merger DWDs have more massive primary WDs, which is similar to the discrepant sample. The observed discrepant sample sharply peaks at $0.6\,M_\odot$, similar to spectroscopic WD mass catalogs (e.g., J. Liebert et al. 2005; P.-E. Tremblay et al. 2016). Our models peak at a similar mass and also contain a peak at slightly larger WD masses (0.7–$0.8\,M_\odot$). The sharp maximum around $0.6\,M_\odot$ is an attribute of the WD IFMR and the IMF. Namely, most IFMRs predict that MS progenitors with masses between 1.5 and 2.0 $M_\odot$ become $0.6\,M_\odot$ WDs (C. E. Fields et al. 2016), and most MS stars that are now WDs had initial masses in this range. This may indicate that observed WDs in this mass range originate from single stellar evolution or from a pre-WD merger that produced a main-sequence star in the 1.5–2.0 $M_\odot$ mass range (e.g., J. Liebert et al. 2005). The observed discrepant systems show a smaller peak around $M_{\rm WD} = 0.8\ M_\odot$, which is consistent with being merger products (e.g., J. Liebert et al. 2005; N. Hallakoun et al.

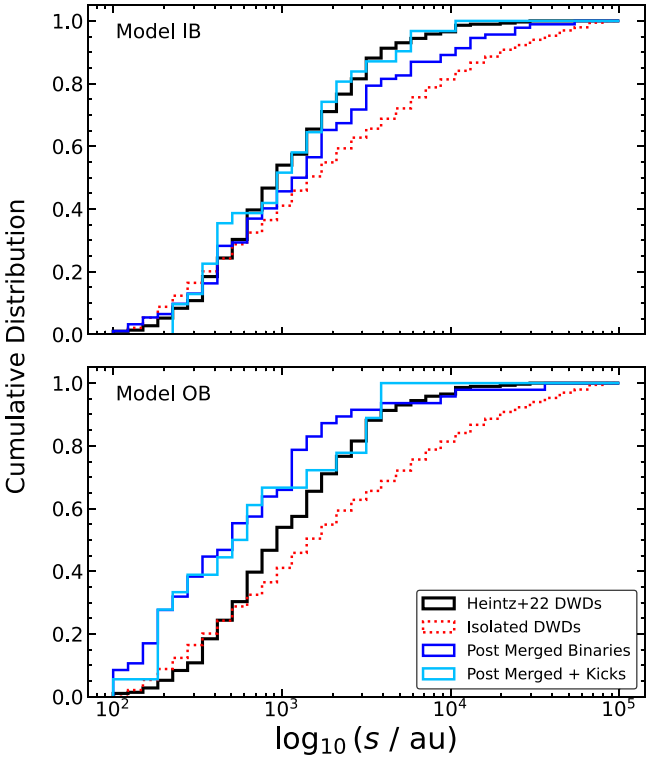

Figure 4. Separation distribution of anomalous DWDs compared to simulations. We show the results of the triples that experienced an inner binary and evolved to be a WD+WD binary at $t = 10$ Gyr. The dark-blue curve assumed no WD birth kicks, and the light-blue systems assumed WDs were born with a small kick. The dotted red line is the distribution for isolated binary evolution using COSMIC population synthesis. The top row shows systems from the IB model, and the bottom panel is derived from the OB model. The Kolmogorov–Smirnov (K-S) test p-values associated with each of these distributions are displayed in Table 2.

2023). In the simulations, we find an additional local maximum at $M_{\rm WD} > 1\ M_{\odot}$, which is not a feature that is observed with Gaia. This feature may be missing from observations because older and cooler WDs are too faint to be seen with Gaia. This high-mass peak may also be an artifact of the COSMIC models, and not be a physical manifestation of mergers (see, e.g., B. M. S. Hansen et al. 2006; P.-E. Tremblay et al. 2016). Also, note that the simulated post-merger masses are heavily reliant on the post-merger mass calculation from COSMIC and our chosen Kroupa IMF.

3.2.2. Separation Distributions

In Figure 4, we compare the separation distribution of our models to those observed by T. M. Heintz et al. (2022). The observed sample (black curve) contains the separations of DWDs from T. M. Heintz et al. (2022) that have anomalous WD ages and have R_chance_align < 0.1, making them confident candidates for bound DWD systems (K. El-Badry et al. 2021). In these DWDs, the more-massive WD exhibits a shorter cooling age than the less-massive WD, with over a 3σ discrepancy (T. M. Heintz et al. 2022, 2024). We also plot the triples in our simulations that had experienced merged inner binaries, leaving a DWD binary that was once a triple (labeled "Post-Merged Binaries"). The top panel of Figure 4 compares the observed distribution to the IB model, while the bottom panel compares it to the OB models. Moreover, for each panel, the light-blue curve shows the same results but accounts for the effect of WD kicks. The separation is generally within a factor of unity with the semimajor axis of the orbit (T. J. Dupuy & M. C. Liu 2011), and for uniform eccentricities, the median conversion factor is $s = a/1.10$. Following this median relation, we plot the scaled semimajor axis of our simulations in this plot. Gaia observations are also susceptible to selection effects, and many DWDs, especially more distant ones, may be missing in the observed sample because they are unresolved. We take into account the selection effects by only including resolved systems in our simulations. Specifically, for each of our simulated DWDs, we sample 100 possible distances based on the distances of the observed DWDs. For each random sample, we calculate whether the system would be resolved at that distance with Gaia's angular resolution of $0\farcs43$ (Gaia Collaboration et al. 2016). If it is resolved for over half the randomly sampled distances, we include it in Figures 3 and 4. Seventy-eight percent of all simulated systems are resolved with Gaia. Note also that many massive WDs are likely missing from the observed sample because they are smaller and, therefore, fainter.

Table 2
Comparison to T. M. Heintz et al. (2022) DWD Distribution

	Model IB	Model IB+K	Model OB	Model OB+K	Binaries
N	101	101	59	59	1625
p-value	0.10	0.76	1.7×10^{-6}	0.35	4.9×10^{-13}

Note. The p-value here is from the K-S test. "+K" denotes WD kicks. See Figure 4 for the distributions.

Additionally, we simulate a population of binaries that become DWDs using COSMIC and compare them to all systems as well (red curve in Figure 4). We choose an initial period distribution from D. Raghavan et al. (2010) with uniform initial eccentricities and a Kroupa IMF. Note that the separation distribution for the binaries is often reflective of the initial separation.

As depicted in the Figure 4, the IB model produces separation distributions that are consistent with the observations, more so than the OB model. Furthermore, the IB model that assumed WD kick has greater consistency with the observed DWDs. The OB systems have a more scattered separation distribution, and since most triples initially had closer tertiaries, the distribution of post-merger DWDs has an abundance of closer systems. We quantify the consistency between the various curves by performing a Kolmogorov–Smirnov (K-S) statistical test with a critical p-value chosen to be 0.05. A K-S p-value below 0.05 would suggest that the two populations likely originated from different parent distributions. Therefore, a larger K-S p-value would indicate that the two distributions were unlikely to come from different parent distributions. We calculate the p-value for all of our models, including our control Binary model, against the observed DWD distribution and display the values in Table 2.

The p-values for the IB models, both without and without kicks, are greater than 0.05, which supports the conclusion that they may come from the same parent distribution. More importantly, the p-value from isolated binary evolution models had a p-value of $\sim 10^{-14}$, making its distribution inconsistent with that of the observed DWD observations. The OB models' p-values are also lower than those from the IB models and are only greater 0.05 when including WD kicks. However, Model

OB also has a smaller number of DWD systems, so their statistical results are less robust. Model IB+WD kicks give the largest p-value of any model, suggesting that it is the closest to the observed distribution.

As discussed in Section 2, the OB and IB models effectively test different methods of early formation of triples. Although they yield a somewhat similar separation distribution (see Figure 1), the OB model assumes that the outer binary formed first, and then the inner binary's orbit was limited by stable configurations allowed by the tertiary. In contrast, the IB model assumed that the configurations of the inner and outer binary are independent under the constraint of dynamical stability. As a result of the different assumptions, the OB models generally contain tighter orbits within the triples for both the inner and outer binary (Figure 1). The distributions in Figure 4 and p-values in Table 2 make it clear that the IB model is far more consistent with the DWD separations in T. M. Heintz et al. (2022) than the OB models. These results suggest that the formation of the inner and outer binary in triples was independent at birth. This corresponds to an independent fragmentation scenario or dynamical capture during stellar formation. Independent hierarchical formation in multiple systems has been supported observationally as well through multiplicity studies (e.g., A. Tokovinin 2014a, 2014b). As a result of the initial sampling, the OB modeling contains more triples with close-by tertiaries. From stability, this also leads to tighter allowed orbits within the inner binary. Considering that the observed DWDs in Figure 4 were originally triples, then we would expect the binaries to have smaller separations ($s \lesssim 10^3$au), which is not observed. The abundance of close-in PMBs produced by the OB model, therefore, renders it inconsistent with the observations (bottom panel), which favor the IB model.

Although both IB models (with and without kicks) exhibit K-S test p-values >0.05, the model that includes kicks has a much larger p-value. The significance of this difference, taken at face value, can provide support for WD kicks. WD kicks widen the separations of DWDs and unbind the widest ones. From the top panel in Figure 4, we find that the kicks caused the cumulative distribution function (CDF) to have a slight peak around $s = 250$ au, which made the rest of the CDF more linear to match observations.

Overall, the IB triple models reproduce the separation distribution of anomalous DWDs significantly better than isolated binary formation and the OB models. This result is statistically robust at 95% confidence because both IB models (with and without WD kicks) have K-S test p-values much greater than 0.05 while the p-value for isolated binary evolution is incredibly small, at 10^{-13}. The triple formation channel not only reproduces the anomalous cooling ages of the observed DWDs (Section 3.2.2) but also reproduces their separations better than isolated binary models. Triple evolution and an agnostic kick mechanism at WD formation provide further evidence for a merger fraction of 21%–36% among wide DWD binaries in the field and a high triple fraction.

4. Stellar Mergers and Blue Stragglers with Companions

4.1. Stellar Mergers and Blue Stragglers Observations

Stellar mergers are common, especially in dense environments (P. J. T. Leonard 1989). One-third of all high-mass MS stars may be merger products (S. E. de Mink et al. 2014). In some cases, mergers manifest as peculiar astrophysical transients. For example, mergers containing WDs may manifest as classical novae (M. F. Bode & A. Evans 2008; S. Starrfield et al. 2016). Mergers containing MS stars can instead be observed as luminous red novae (RNe; N. Soker & R. Tylenda 2006; R. Tylenda & N. Soker 2006; N. Ivanova et al. 2013; O. Pejcha et al. 2016; M. MacLeod et al. 2017; B. D. Metzger & O. Pejcha 2017; T. Matsumoto & B. D. Metzger 2022). RNe are a class of transients characterized by their large energy output (10^{45}–10^{47} erg), which is just below that of Type Ia supernovae (H. E. Bond et al. 2003; S. R. Kulkarni et al. 2007). One example of an observed merger is the case of V1309 Sco (R. Tylenda et al. 2011), which was the first LRNe to be observed before, during, and after its final moments. V1309 Sco started as a contact binary with a 1.4 day period, and over time, its period decreased until the two stars merged and the RNe formed (R. Tylenda et al. 2011).

BSSs are stars found to be bluer or brighter than the main-sequence turnoff. BSSs are most often identified in clusters that have known ages derived from their color–magnitude diagrams. BSSs are predicted to be the result of mass transfer or a collision between two MS stars (e.g., J. Lombardi et al. 1995; J. C. J. Lombardi et al. 1996; P. J. T. Leonard 1989; A. Sills et al. 1997, 2001; A. Sills et al. 2002, 2005; M. Freitag & W. Benz 2005; N. Ivanova et al. 2008; H. B. Perets & D. C. Fabrycky 2009; N. M. Gosnell et al. 2014; S. Naoz & D. C. Fabrycky 2014). BSSs can also be the result of the interaction or merger between an MS star and an evolved companion (W. H. McCrea 1964; X. Chen & Z. Han 2008; R. D. Mathieu & A. M. Geller 2009; N. M. Gosnell et al. 2019; A. C. Nine et al. 2020). Another class of BSSs with similar formation histories are "blue lurkers" (BLs), which are identified by their anomalously fast rotation rates (E. Leiner et al. 2019). Their rapid rotation makes them strong candidates for a prior merger event (A. Sills et al. 2001; B. W. Carney et al. 2005; A. Sills et al. 2005). The rotation also extends their lifetime as a BSS due to the rotational mixing (e.g., A. Sills et al. 2005; E. Glebbeek & O. R. Pols 2008). Other observations of peculiar stars include yellow straggler stars (S. E. Strom et al. 1971), which lie between the end of the MS and the red giant branch (RGB; hypothesized to be evolved BSSs), and red straggler stars (A. M. Geller et al. 2017), which are redder than the RGB. We do not study these in detail here, though our discussed mechanisms may apply to their formation as well.

Observations of star clusters have revealed that BSSs are 2–4 times more likely to contain a companion relative to regular MS stars (e.g., R. D. Mathieu & A. M. Geller 2009; A. M. Geller & R. D. Mathieu 2012; A. C. Nine et al. 2020). In the NGC 188 and M67, which have some of the most well-studied BSS populations, the binary fraction of BSSs is of $\sim 76\% \pm 19\%$ and $\sim 79\% \pm 24\%$, respectively (e.g., R. D. Mathieu & A. M. Geller 2009; A. M. Geller & R. D. Mathieu 2012; A. M. Geller et al. 2015). The companions to BSSs are observed at periods ranging from 1–10,000 days and eccentricities ranging from 0 to ~ 0.9 (e.g., R. D. Mathieu & A. M. Geller 2009; A. M. Geller & R. D. Mathieu 2012; A. M. Geller et al. 2015). The observed eccentric orbits disfavor isolated binary formation channels since the mass transfer would have presumably circularized the orbits, or they require an additional eccentricity pumping mechanism. If mass transfer between an MS star and an AGB donor did not cause the progenitors to merge, the post-common envelope binary could manifest as a blue straggler

binary with a hot C/O WD companion (R. Kippenhahn et al. 1967; D. Lauterborn 1970; B. Paczyński 1971; Y. Zenati et al. 2019). Such BSSs with hot white dwarf companions have been observed, especially as of recent (e.g., N. M. Gosnell et al. 2014, 2019; V. V. Jadhav et al. 2021; S. Pandey et al. 2021; M. Sun et al. 2021; K. Vaidya et al. 2022; A. C. Nine et al. 2023).

The UV-bright WD companions observed nearby in BSSs are a potential marker for a mass transfer history and not a stellar merger. Also, the fact that most BSSs have nearby companions (<1000 days) may also lend support to them being the outcome of mass transfer. However, the binary mass transfer channel has a few difficulties. First, observations of some BSSs with low-mass WD companions show that the stars were expected to have undergone unstable mass transfer based on their observed characteristics (e.g., S. Pandey et al. 2021). Second, many BSS binaries are eccentric. These difficulties could be resolved with the three-body channel. If BSSs are formed through the merger channel, their observed companion would be the tertiary star from the triple. In this case, the observations are actually of the outer binary, which would explain the high eccentricities and the formation of a WD companion in a closer orbit. Namely, the detected WDs could be unresolved inner orbits (S. Pandey et al. 2021). In a triple formation history, the inner binary experiences Kozai–Lidov cycles, which oscillate the eccentricity and inclination of the inner binary (S. Naoz 2016). During high eccentricity excursions, the pericenter distance decreases, making the probability of stellar interaction high. Collisions induced by destabilized triples can also contribute to their formation, albeit with lower rates (S. Toonen et al. 2022).

Previous studies have investigated the formation of BSSs from hierarchical triples, (e.g., H. B. Perets & D. C. Fabrycky 2009; S. Naoz & D. C. Fabrycky 2014), but neglected single and binary stellar evolution. Here, we invoke our simulations of three-body systems—which include triple dynamics, single stellar evolution (with SSE), and detailed binary interactions (with COSMIC)—to study BSSs. Specifically, we seek to understand whether the merger channel can still support a fraction of observed BSSs. In Section 4.2 we apply our simulated triples that experienced an MS+MS or RG+MS merger to investigate the formation and future evolution of BSSs with companions. We compare these theoretical systems to observations of BSS binaries in the field from B. W. Carney et al. (2005), BSS binaries in M67 from D. W. Latham (2007), BSS binaries in NGC 188 from A. M. Geller et al. (2009), and BLs in M67 from E. Leiner et al. (2019).

4.2. Comparing Observed Blue Stragglers to Theoretical Simulations

4.2.1. Formation from MS+MS and RG+MS Mergers

To identify BSS binaries from our simulations, we take the systems where the inner binary began to transfer mass between two MS stars or one MS and one RG star (which includes stars on the AGB). We then follow the detailed mass transfer evolution in COSMIC and only consider those that merge entirely, leaving one MS remnant star behind. We interpret this rejuvenated star as a BS (or BL) star. The triple has now become a binary, where the newly formed primary star is the rejuvenated merger product of two MS stars or an MS+RG, and the secondary is the original tertiary star from the old triple system (often an MS star). We seek to understand how this BSS binary evolves over different timescales after the merger. At the time of the merger, there are 491 binaries: 237 from the OB model and 254 from the IB model. In total, 63% were RGMS mergers, and the rest were MSMS. Most (65%) of RGMS mergers merged in their progenitor triple after 1 Gyr of three-body evolution, while this is only the case for 16% of MSMS mergers. However, 79% of MSMS mergers occurred after 100 Myr of triple evolution, and 34% occurred after 500 Myr. In total, 91% (446/491) of the MSMS/RGMS inner binaries merged after 100 Myr with 47% (228/491) merging after 1 Gyr of three-body evolution. Previous studies of BSS formation from triples found that inner binaries will merge and produce a BSS very rapidly ($\lesssim 10^7$ yr; H. B. Perets & D. C. Fabrycky 2009; S. Naoz & D. C. Fabrycky 2014). These models struggle to reproduce the old BSS populations in clusters (e.g., A. M. Geller et al. 2015) and even the field BSSs (e.g., B. W. Carney et al. 2001) because the stars would merge too early and their product would not be observable as a BSS today. With our inclusion of stellar evolution and detailed mass transfer evolution, most merger events occur much later in the evolution of the triple, making the three-body formation channel viable.

After the inner binary merged and the BSS presumably formed, we evolve the rejuvenated BSS binaries for different amounts of time after the time of merger ($t_{\rm merge}$). In Figure 5, we show how the period and eccentricity change for these binaries after 10 Myr, 50 Myr, and 100 Myr of PMB evolution using COSMIC.[6] Here, we show the systems that remained on the MS after the merger and discard those that become WDs. At 100 Myr post-merger, 22% of the merger products have become WDs (see Appendix A). The maximum BSS lifetime is assumed to be around 1–2 Gyr (A. Sills et al. 2009). From 100 Myr to 1 Gyr post-merger, once tides have settled, the binary orbits do not change significantly, and most BSSs (80%) become WDs. To understand how the MSMS and MSRG merger systems evolve for longer timescales, including post-WD formation, see Figure 7 in Appendix A.

In Figure 5, the squares represent MSMS mergers, and the circles correspond to RGMS mergers. The color of the points corresponds to the evolution time. In the top panel, we show the orbital structure at the instant that the inner binary completely merged within the triple: the time that the triple became a BSS binary. The circular points often have a darker shade than the squares because the RG+MS binaries generally merge later than the MS+MS mergers. To the right of each period–eccentricity diagram, we show the eccentricity probability density for the MS+MS merger (light blue) and RG +MS mergers (navy blue). Furthermore, we plot the points for observed BSSs and BSS-like systems in black with a red outline. All of the black points are observed systems that are likely to be binaries, with one component being the remnant of an MS+MS or RG+MS collision event. The triangles are the observations of BSS binaries in the field (B. W. Carney et al. 2005), the pentagons are BSS binaries in M67 from D. W. Latham (2007), and the diamonds are BL binaries in M67 (4 Gyr, turnoff mass 1.3 $M_\odot$; L. Balaguer-Núñez et al. 2007) from E. Leiner et al. (2019). The black circles are BSS binaries in NGC 188 (7 Gyr, turnoff mass 1.1 $M_\odot$; A. Sarajedini et al. 1999; from A. M. Geller et al. 2009; R. D. Mathieu &

[6] Note that COSMIC assumed efficient tidal evolution (rapid $e = 0$ for tight binaries; K. Breivik et al. 2020a), which underestimates the eccentricity for these systems.

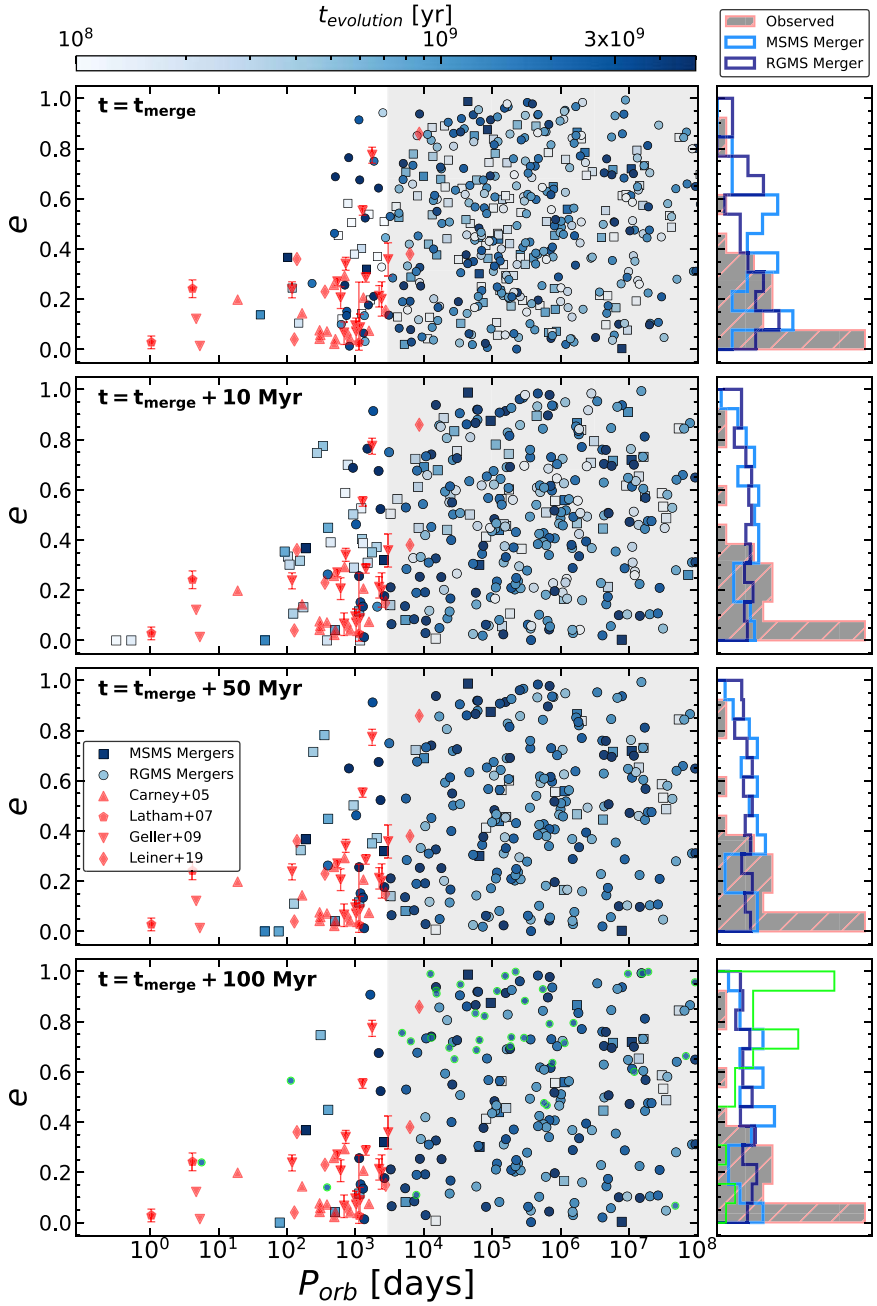

Figure 5. Period–eccentricity diagram of triple systems that experienced an MSMS or RGMS inner binary that merged at different points after the merger time. After the inner binary merges, the triple becomes a PMB. Here, we plot the period–eccentricity diagram for this new binary at the time of the merger (top panel), 10 Myr after the merger (second panel), 50 Myr after the merger (third panel), and 100 Myr after the merger (fourth panel). If the merger product evolves into a WD, we remove it from the subsequent panels. In red, we overplot observations of blue straggler binaries in the field from B. W. Carney et al. (2005), blue straggler binaries in M67 from D. W. Latham (2007), blue straggler binaries in NGC 188 from A. M. Geller et al. (2009), and blue lurkers (BLs) in M67 from E. Leiner et al. (2019). In the first panel only, we color the points by the evolution time at the moment that they merged, $t_{\rm merge}$. To the right of every scatter plot, we show the probability density distribution of the simulated MSMS mergers (blue) and RGMS mergers (purple) and compare them to all of the observations (gray-hatched distribution). The shaded region is undetectable by the WOCS RV survey (A. M. Geller et al. 2021).

A. M. Geller 2009; A. M. Geller & R. D. Mathieu 2012). The eccentricity distribution for the observed BSS binaries is also shown (gray-hatched distribution).

In the bottom panel, the green points are the simulated systems that included the impact of WD kicks for each WD companion formed during the $t = 100$ Myr post-merger evolution. The adjacent lime histogram shows the distribution of systems with WD kicks. In general, the stellar type of the secondary companions from the observations is unknown, so the fraction of WDs in the observational sample is also unknown. However, the secondary mass distribution of BSS binaries with ∼1000 day periods in NGC 188, as determined through kinematic fitting, peaks at ∼0.5 $M_\odot$ (A. M. Geller & R. D. Mathieu 2011). This may suggest that WD companions are common. In Appendix B, we show the secondary mass distributions of our simulated BSS binaries with $P_{\rm orb} <$ 5000 days compared to BSS binaries in NGC 188 (A. M. Geller & R. D. Mathieu 2011) with similar periods. In general, we find peaks around 0.5–0.75 $M_\odot$ for the BSS companion, consistent with A. M. Geller & R. D. Mathieu

(2011). In our BSS binaries with $P_{\rm orb} < 5000$ days, the companion is a low-mass MS star 87% of the time and a WD 13% of the time 10 Myr post-merger. After 100 Myr post-merger, 25% of the BSSs have WD companions.

Since WDs are abundant in BSS systems, we include the systems that experienced small recoil kicks after WD formation to show how kicks affect their eccentricities and periods. As seen from the bottom panel of Figure 5, the binaries with WD kicks achieve wider orbits with higher eccentricities ($e \sim 0.8$). Also, most of the close-in systems ($P_{\rm orb} \lesssim 10^4$ days) reach wider orbits, and most of the wide orbits become unbound. Nearly all of the observations of BSS binaries were taken using the WOCS radial velocity survey, which has a maximum period detection limit of 10^4 days (A. M. Geller & R. D. Mathieu 2012; A. M. Geller et al. 2021), with most being under 3000 days. Despite this bias, we plot all of our systems over a wide period to give an example distribution for the parent population of BSS binaries.

4.2.2. Origin of the Orbital Structure of BSS Binaries

At $t_{\rm merge}$, the three-body merger channel can successfully reproduce the orbital architectures of most systems, except the shortest BSS binaries. Notably, observed systems with periods above 10 days have periods and eccentricity that bode well with having previously been hierarchical triples. At this period range, the observed BSS binaries in NGC 188 (A. M. Geller et al. 2009) have a roughly uniform eccentricity distribution, similar to what is expected from the merger channel. On the other hand, the combined observations have a slight preference for smaller eccentricities ($e < 0.5$) at this period range. These systems are closely similar to the RGMS mergers with similar periods of ∼1000 days but also are consistent with being post-common envelope binaries at this period range (N. Yamaguchi et al. 2024a). The preference for shorter eccentricities at these periods may also be a marker for a mass-transfer history within an isolated binary. Among the observed BSS binaries with $P_{\rm orb} < 1000$ days, most have nonzero, moderate eccentricities. This is surprising considering that they would have presumably circularized rapidly during their mass transfer evolution. A similar phenomenon is observed in post-common envelope binaries with similar periods (N. Yamaguchi et al. 2024a). For BSSs, this challenges the mass transfer formation channels and may indicate that another mechanism is pumping eccentricities.

One eccentricity pumping mechanism to account for the tight BSS binaries with moderate eccentricities is WD formation kicks. When including the impact of WD kicks, we find that one of our short-period ($P_{\rm orb} < P_{\rm circ}$) BSS binaries with a WD companion escaped its circular orbit and became eccentric upon WD formation (bottom panel of Figure 5). Since the orbit is consistent with observations, kicks from WD companions can provide a method of explaining the eccentricities of tight BSS binaries. If this is true, we would predict that BSS binaries with orbital periods less than the circularization period and with nonzero eccentricities have WD companions. This scenario is already supported by observations from calculations of secondary masses to BSSs (A. M. Geller & R. D. Mathieu 2011) and observations of hot WDs nearby BSSs (e.g., N. M. Gosnell et al. 2014, 2019; V. V. Jadhav et al. 2021; M. Sun et al. 2021; K. Vaidya et al. 2022; A. C. Nine et al. 2023).

The eccentricity could also be attributed to a distant tertiary that is exciting the eccentricity of the system or cluster dynamics. The tertiary star in a hierarchical triple can still excite eccentricities within inner binaries that have periods around 10 days if the inner binary contains a WD. For example, C. Shariat et al. (2023) showed that noninteracting WD+MS inner binaries with separations of 0.1 au ($P_{\rm orb} \sim 10$ days) contain a wide range of eccentricities when they are in hierarchical triples. Moreover, the companions to these binaries have separations between 10 and 10^4 au. Therefore, some BSSs binaries may also contain a tertiary as far as 10^4 au away. Note that the currently observed companion could also be the tertiary.

From COSMIC, an MS+MS merger generally manifests as one inflated MS star, which would have highly efficient tides and an assumed zero eccentricity. Notably, some of the MSMS merger systems sparked a short period of mass transfer during their inflated state or later on as the tertiary evolved off the MS. The latter scenario is the same as shown on the right side of Figure 2. Such a scenario is an example of triple (or tertiary) mass transfer, which has been noted previously (Y. Gao et al. 2023; A. Dorozsmai et al. 2024; A. C. Nine et al. 2024), and we find here that it can be a fascinating channel to form close-in BSS binaries.

A significant fraction of BSS stars have observed barium enrichment (A. C. Nine et al. 2024), which is a signature of AGB mass transfer. However, if most BSSs are formed from AGB mass transfer, BSS binaries with $P_{\rm orb} \gtrsim 1000$ days are expected to be rare since unstable mass transfer would lead to a merger or a tighter orbit. If we consider that the Ba enrichment is from an AGB+MS merger, which is the scenario for most of the RG+MS mergers, these orbital periods would be attainable. We discuss the AGB merger scenario more below.

As mentioned, a distinct sign that a star transferred mass or merged with an AGB companion is the enrichment of *s*-process elements such as barium (Ba; I.J. Iben & A. Renzini 1983; M. Busso et al. 1999). A. C. Nine et al. (2024) found that $43\% \pm 11\%$ of the BSSs that they observed in three different clusters, including M67, are Ba enriched. Many Ba-enriched stars have observed companions (A. Escorza et al. 2019; A. Jorissen et al. 2019; A. C. Nine et al. 2024), most of which are WDs. Most Ba binaries have orbital parameters consistent with AGB mass transfer, though some exhibit puzzling configurations. Namely, a handful of "unexplained" Ba-enriched binaries have been discovered (A. Escorza et al. 2019; A. Jorissen et al. 2019) at periods that cannot be reproduced with binary evolution modes. Three of these binaries have short periods ($P_{\rm orb} < 700$ days) but modest eccentricities (A. Escorza et al. 2019), and two have a long period ($P_{\rm orb} \sim 10^4$ days) and very high eccentricity ($e \gtrsim 0.9$; A. Escorza et al. 2019; A. Jorissen et al. 2019). If we consider that the Ba enrichment is from an AGB+MS merger, which most of our RG+MS mergers are, then these orbital periods can be abundantly formed with the triple-merger channel (Figure 5, top panel). As discussed earlier, the unexplained short-period Ba-enriched binaries could have a similar formation to the close-in, eccentric BSS binaries that we describe above. Also, since these Ba stars have WD companions, kicks could play a role to slightly alter eccentricities. The long-period "unexplained" binaries are occupied in the eccentricity–period diagram in Figure 5, especially by RG+MS mergers in triples in the top and bottom panels. Previous studies also support that a significant fraction of Ba stars may have formed from hierarchical triples (Y. Gao et al. 2023).

Overall, we find that the triple+merger channel can reproduce the periods, eccentricities, and many other discussed characteristics of most observed BSS binaries. However, observations of BSS binaries clearly show that ∼75%–80% of them have companions with orbital periods <3000 days (A. M. Geller & R. D. Mathieu 2011; A. M. Geller et al. 2015). In the triple+merger channel, most tertiaries lie at periods above this range and beyond the RV detection limit of the BSS surveys, making them observable as single BSSs. Therefore, for BSS binaries with periods below 3000 days, the stable mass transfer channel is likely to be dominant. Nevertheless, there exists a handful of observed BSS binaries with peculiar properties in this period regime that can be naturally explained by the triple+merger channel or by accounting for additional binary evolution mechanisms. Furthermore, based on our models, it is likely that the 20%–25% of BSSs without nearby companions formed via the triple+merger channel and have tertiary stars beyond the detection limit. Previous studies have estimated that the fraction of BSSs formed in triples is closer to 10% (F. Antonini et al. 2016). Lastly, it is important to note that mass transfer will not always lead to circular orbits, which is a feature of COSMIC models (e.g., A. S. Hamers & T. A. Thompson 2019).

5. WD+MS and WD+RG Merged Inner Binaries

A quarter of all merged triples include mergers between a WD +MS or WD+RG (Table 1). Before the WD formed, many of these inner binaries already experienced a common envelope phase. For most of the WD+RG mergers, the first mass-transfer episode stopped when the WD formed, and the second mass-transfer episode (which led to the merger) began as the secondary reached the first RGB or AGB. Here, we are interested in the triple's orbital configuration at the onset of mass transfer with the WD primary. In Figure 6, we plot the parameter space for the orbital periods in the triple at the onset of WD mass transfer. We denote the inner (outer) period at the onset of WD mass transfer as $P_{1,\mathrm{onset}}$ ($P_{2,\mathrm{onset}}$). In the WD+MS mergers, we also include companions that are in the Hertzsprung Gap.

In general, the RG stars begin mass transfer at larger $P_{1,\mathrm{onset}}$ since they have larger radii. At the onset of WD mass transfer, the inner periods are bimodal for both WD+MS and WD+RG systems. This bimodality is especially pronounced for the WD +RG accreting binaries and can provide clues to their formation history. All of the short-period WD+RG binaries ($P_{1,\mathrm{onset}} < 10$ days) have C/O WDs, whereas most of the longer-period ones have He WD primaries. The WD type gives insight into how the WD progenitor evolved, and when it began its first (pre-WD) common envelope evolution. For example, most of the He WDs progenitors began mass transfer earlier than the C/O WD progenitors, meaning their envelopes were stripped earlier from the secondary. Furthermore, C/O WDs generally have smaller radii than He WDs, so they only initiate mass transfer with larger, more evolved companions.

All of these mass transferring WD+MS and WD+RG in Figure 6 eventually merged. During the pre-merger mass transfer, the WD+MS binaries would be observed as a CV-like system with a gradually decreasing period. For low-mass WDs, WD+MS merged systems are expected to be a common outcome from their unstable common envelope evolution. This merger scenario could potentially account for the abundance of high WD masses and the lack of He WD accretors in CVs

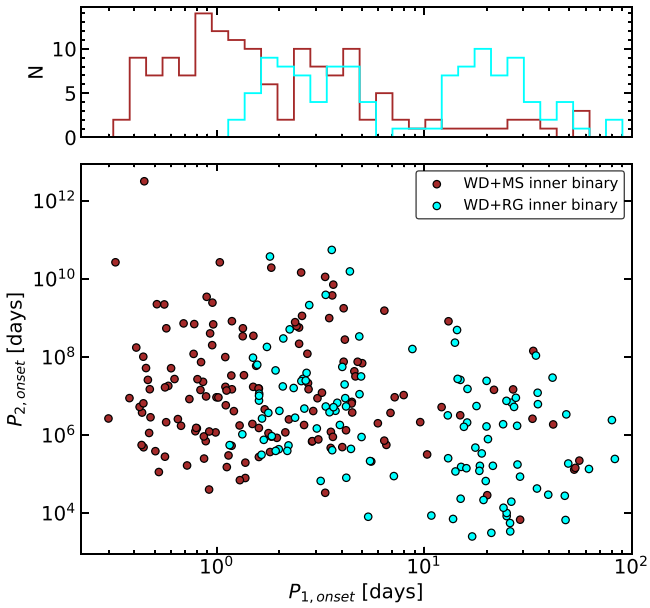

Figure 6. The inner and outer period in the triples with inner merged WD+MS (red) or WD+RG (cyan) binaries at the onset of WD mass transfer ($P_{1,\mathrm{onset}}$ and $P_{2,\mathrm{onset}}$, respectively). In the top panel, we plot the unnormalized distribution of $P_{1,\mathrm{onset}}$ for both types of inner binaries.

(M. R. Schreiber et al. 2016; D. Belloni et al. 2018). Namely, the lower-mass WDs would have led to a quick merger and failed to produce a CV. From the abundance of high-mass WDs in CVs, it is therefore expected that a population of WD+MS merger products, or "failed CVs," exist in the Galaxy. These merger remnants are expected to look like a modified RG star with a dense core and an inflated envelope generated from the MS component (N. Z. Rui & J. Fuller 2024). In fact, most of the WD+MS merger products from our simulations lie on the RGB, according to COSMIC. These unusual RG stars may exhibit distinct photometric, asteroseismic, and surface abundance signatures (N. Z. Rui & J. Fuller 2021; S. Deheuvels et al. 2022; Y. Li et al. 2022; M. Matteuzzi et al. 2023; N. Z. Rui & J. Fuller 2024).

6. Other Outcomes

6.1. Double Mergers

After the inner binary merges in a hierarchical triple, a PMB is formed, and in 10% of all simulations, the PMB also experiences mass transfer evolution. One example of common envelope evolution in a PMB is displayed in Figure 2. Interestingly, in 4.4% (36/810) of all PMBs, the PMB underwent unstable mass transfer and merged again, leaving behind a single star. These systems began as hierarchical triples; the inner binary merged, and then the remaining binary merged, leaving *a single* star behind. This "double merger" scenario occurred 36 times in our simulations and possesses a diverse array of formation histories and potential future evolution. Among the double mergers, the first inner binary merger was between an MS+MS, RG+MS, and WD+MS in 26 (72%), six (27%), and four (11%) cases, respectively. For all four WDMS inner binary mergers (which left behind a single WD), the second merger was also a WD +MS merger. Since this post-merger, WD was already massive ($\gtrsim$0.8 $M_\odot$), in all four cases, the second merger event ignited a super-Chandrasekhar explosion, which did not leave behind any remnant star. The commonality of such an explosion from the

double merger channel is unknown, though observations suggest that many local massive WDs may be merger products (N. Hallakoun et al. 2023). Moreover, we showed earlier (Section 3) that many field WDs in wide DWDs experienced a prior merger (Section 3). With a considerable number of post-merger massive WDs from triples, the double merger channel may be a notable method of producing single-degenerate Type Ia supernovae in the Galaxy. In observations, double mergers will likely be difficult to distinguish from single mergers. Similar to single mergers, double mergers may contain photometric, asteroseismic, and surface abundance features (e.g., N. Z. Rui & J. Fuller 2021), though future work is required to disentangle them from regular stars and single mergers.

6.2. Neutron Stars from Mergers

Another interesting, yet small (2%, 18/810), subset of our merged systems comprises those that produced a neutron star (NS) in the PMB after 10 Gyr of total evolution time. This includes an NS+MS, NS+RG, and NS+WD binaries. Initially, the masses from the Kroupa IMF were constrained to be below 8 $M_\odot$ (C. Shariat et al. 2023), so producing an NS requires either an MS progenitor >8–10 $M_\odot$ (which must have formed from a previous merger or mass transfer) or an accretion-induced core-collapse of a WD. Nine of the binaries did not remain unbound after the neutron star supernova kick. Two of them remained bound but later merged because of their high post-kick eccentricity, leaving behind one NS. Of the seven surviving NS binaries (six with MS companions and one with a WD companion), one formed from accretion-induced WD collapse, and the rest became massive stars after previous episodes of mass transfer or a previous merger. The separations of the NS +MS binaries from this channel range from 100–3000 au, while the two NS mergers were short-lived at $\lesssim$1 au eccentricities.

In general, the NS in NS+MS binaries formed after two ~5 $M_\odot$ MS stars in the inner binary coalesced with minimal mass loss to produce a rejuvenated ~10 $M_\odot$ star on the MS, which later evolved into an NS. Previous simulations support that little mass is lost during MS+MS mergers (J. C. J. Lombardi et al. 2002; J. E. Dale & M. B. Davies 2006; E. Glebbeek & O. R. Pols 2008). Before WD formation, this rejuvenated massive star may exhibit a strong, large-scale magnetic field (e.g., J. F. Donati & J. D. Landstreet 2009; L. Ferrario et al. 2015; L. Fossati et al. 2015; F. R. N. Schneider et al. 2016) that hints at its merger origin.

The NS+WD PMB formed as the result of a WD further collapsing into an NS after mass transfer with a donor. In the original triple, two MS stars merged to create one 7 $M_\odot$ MS star in a binary with a 1 $M_\odot$ MS star. As the primary MS star evolved, mass transfer began, and it eventually became a 1.3 $M_\odot$ Ne/O WD. Then, as the secondary evolved, the two stars began common envelope evolution, which led to the WD collapsing into an NS. The NS is also a pulsar rotating 400 times per second while the secondary is a 0.1 $M_\odot$ He WD. The supernova induced a 40 km s^{-1} kick, making the final orbital period of the NS+WD binary only 100 minutes. During the evolution of this binary, it may have been observed as a CV (during the MS accretion onto the WD), and at its final configuration, would possess signatures as a millisecond pulsar with strong gravitational wave emission from its nearby WD companion (observed examples in the ATNF pulsar catalog; R. N. Manchester et al. 2005). Eventually, gravitational waves will extract energy from the binary, which will shrink the orbit and eventually put the two stars in contact. In this binary, the WD mass is small enough ($\lesssim$0.2 $M_\odot$) such that the NS+WD mass transfer will be stable (A. Bobrick et al. 2017), making the system an ultra-compact X-ray binary (L. M. van Haaften et al. 2012).

NS binaries were not the primary focus of this study. However, their formation from solar-type triples presents an intriguing scenario for creating close, intermediate, and wide NS binaries. Intermediate-separation NS binaries have been observed with Gaia (e.g., J. J. Andrews et al. 2022; K. El-Badry et al. 2024a, 2024b). Moreover, the triple channel proved to form close NS binaries with MS and WD companions, which can be observed as symbiotic X-ray binaries (e.g., K. H. Hinkle et al. 2006; K. H. Hinkle et al. 2019, 2024; L. R. Yungelson et al. 2019; P. Nagarajan et al. 2024) during their evolution. Future work that focuses on larger initial masses can examine the efficiency of the triple-merger channel in forming NS binaries.

7. Conclusions

Over the past decades, observations of stars have challenged our understanding of single stellar evolution and often required the consideration of binary and higher-order systems to explain their formation. Fortunately, most stars form and evolve with one or multiple stellar companions (D. Raghavan et al. 2010; M. Moe & R. Di Stefano 2017), making stellar interactions highly probable. Previously, C. Shariat et al. (2023) evolved solar-type triples for over 10 Gyr using detailed dynamical simulations with stellar evolution. In their simulations, more than half of all solar-type triples experience inner binaries that merge within 12.5 Gyr. In this study, we focus on investigating the formation and evolution of stellar triples with merged inner binaries containing main-sequence, red giant, and white dwarf stars. Specifically, we explored the outcomes of merged MS +MS, RG+MS, WD+MS, and WD+RG merger inner binaries.

On top of the dynamical simulations, we track the detailed mass transfer history in these triples using the `COSMIC` binary stellar evolution code. This includes the first episode of mass transfer, which led to a merged inner binary, and the subsequent evolution of the PMB. Often, we evolve the PMB for megayears to gigayears after the merger event. We then compare our results to the observation of peculiar stellar systems to examine the following question: does a PMB retain any signature of its triple past?

Throughout this paper, we discussed the different potential outcomes of PMBs and compared them to observations of wide DWDs and BSS binaries to test the three-body formation channel. Our main results are summarized as follows:

1. *Triple formation channel for DWD binaries.* We find strong evidence that DWD binaries with discrepant ages (T. M. Heintz et al. 2022, 2024) are the result of previous triples that experienced a merger. In particular, we show that the triple-merger channel reproduces the discrepant ages (Figure 3) and the separation distribution of observed DWDs, whereas isolated binary evolution cannot (Figure 4 and Table 2). The model that matched most closely with the observations was IB+kicks, which assumes that an agnostic mechanism causes a small ~0.75 km s^{-1} kick in the system. Presumably, kicks are a result of asymmetric mass loss during WD formation. The kicks fundamentally shift the separations of the simulated binaries to create a greater statistical match.

This provides further support for the existence of WD recoil kicks.

2. *Formation hierarchy in stellar triples.* Our triple models that assumed independent orbital periods between the inner and outer binary are consistent with observations of wide DWDs, while our other model is not (Figure 4 and Table 2). The consistency between the IB model and observations gives insight into the order of star formation during the early phases of multiple stellar evolution. Namely, it supports a scenario where the inner binary and the tertiary form independently and at roughly the same time.
3. *Significant merger fraction in wide DWD binaries.* The strong consistency of the triple channel with anomalous DWDs suggests that 26%–54% (T. M. Heintz et al. 2022) of wide DWDs were previously three-body systems, and today, the more-massive WD is a merger product. Another fraction of DWDs previously had a companion that was made unbound due to flyby stars, and WD kicks over 10 Gyr of evolution (e.g., C. Shariat et al. 2023). Sixty-one percent of the simulated triples from C. Shariat et al. (2023) that formed a DWD became unbound from the tertiary, and out of all of the initial triples, 14% became isolated DWD binaries with $s > 100$ au. Assuming that 30% of all solar-type stars ($<8\ M_{\odot}$) were born in triples (C. Shariat et al. 2023), then 4% of all solar-type stars become isolated DWDs after unbinding with a tertiary. In total, we estimate that $44\% \pm 14\%$ of local DWDs were birthed in triple-star systems and are now isolated binaries because of a previous merger or because they became unbound with a prior companion.
4. *Formation channel for BSS binaries.* The orbital configuration of PMBs that had MSMS or RGMS mergers closely matches with most ($P_{\rm orb} > 10$ days) observed BSS binaries (Figure 5). Based on this, we predict that the 20%–25% of BSSs without nearby companions formed via stellar collisions and have very long-period ($P_{\rm orb} > 3000$ days) companions. However, current observations show that most observed BSSs in clusters have close companions ($P_{\rm orb} < 3000$ days; A. M. Geller & R. D. Mathieu 2011; A. M. Geller et al. 2015), which supports that a majority of BSSs formed via stable mass transfer. Still, the eccentricities in some of the close BSS binaries are inconsistent with stable mass transfer, but can naturally be explained by triple dynamics or by considering an additional eccentricity pumping mechanism (e.g., WD kicks). We also show that collisions in hierarchical triples often occur after megayears to gigayears of triple evolution, producing BSS ages consistent with old clusters. Lastly, similar to the mass transfer channel, the triple+merger channel would also produce enriched chemical abundances, fast rotation rates, and companion masses observed in many BSSs.
5. *Signatures of WD Formation Kicks.* We find imprints of WD recoil kicks consistently throughout our analyses. In the case of DWDs, WD kicks serve to qualitatively change the modality and shape of the separation distributions. They create a bimodal distribution, leading to a greater statistical consistency between theory and observations. In the case of BSS binaries, WD kicks lead to an explanation for the eccentric short-period binaries observed, which would, therefore, presumably have a WD companion. The eccentricity can also be attributed to a distant, unresolved tertiary (see Section 4.2) or cluster dynamics.
6. *WDMS and WDRG mergers.* We find that 19.8% (7.1%) of PMBs formed after a WDMS (WDRG) merged inner binary. Figure 6 depicts the inner and outer periods of hierarchical triples with merged WDMS and WDRG inner binaries. The inner periods are plotted at the first moment of WD mass transfer (Figure 6), which initiates an unstable interaction and leads to their eventual merger. These mergers are expected to produce CV-like systems and transient novae (see Shariat et al. in prep for more details).
7. *Other Outcomes.* We show that triples with mergers can also provide a formation channel for close, intermediate, and wide NS+MS or NS+RG binaries. In this channel, the NS either formed from an MS progenitor that became a massive star after a merger or from accretion-induced WD collapse. We also explore triples that experience two mergers (5% of PMBs), which provide a method of producing single-degenerate Type Ia supernova. Understanding the dynamical origins and identifying formation markers of merged stars is increasingly important, especially as methods of distinguishing merger remnants from regular stars continue to advance.

Acknowledgments

We thank Tyler M. Heintz and J.J. Hermes for bringing to our attention the age-discrepant DWDs in the Gaia sample. We thank the anonymous referee for providing a constructive report. This work used computational and storage services associated with the Hoffman2 Shared Cluster provided by UCLA Office of Advanced Research Computings Research Technology Group. S.N. acknowledges the partial support from NASA ATP 80NSSC20K0505 and from the NSF-AST 2206428 grant, as well as thanks Howard and Astrid Preston for their generous support.

Appendix A
The Long-term Evolution of MS+MS and RG+MS Mergers

After 100 Myr post-RG+MS merger, most of the merger products have evolved to WDs. In this case, the merger product is too evolved to be a bright star on the MS, so it will not be observable as a BSS. In Figure 7, we show the orbits of these evolved PMBs as the merger product evolves to a WD. In most cases, the PMB circularized as the progenitor of the WD, which is the merged star, evolved off the main sequence. The post-merger evolution is dependent on `COSMIC` models. For details on the evolution of BSSs that formed through stellar mergers, see Section 4.

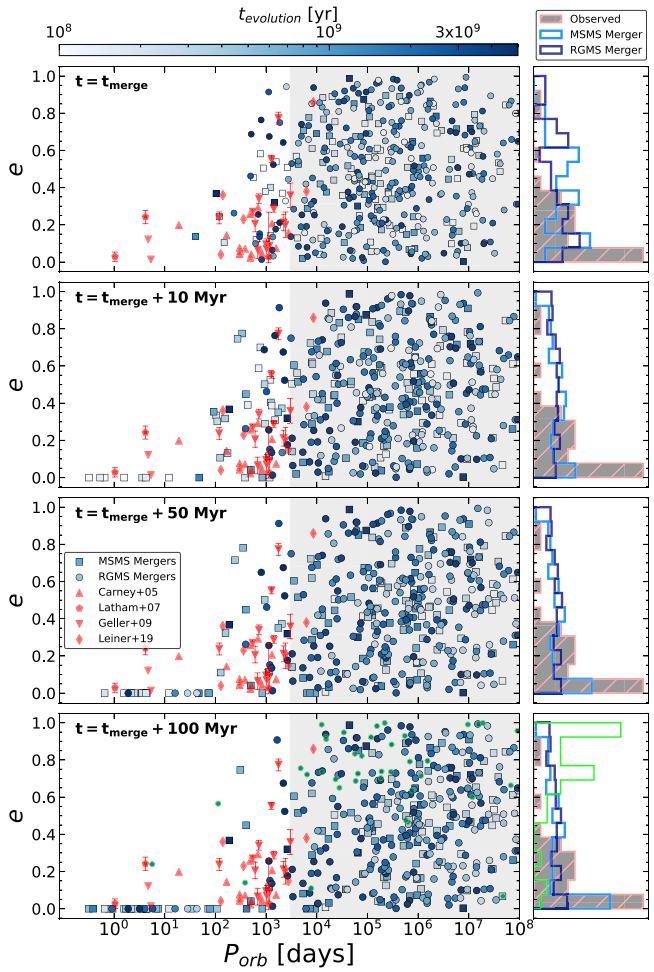

Figure 7. Period–eccentricity diagram of triple systems that experienced an MS +MS or RG+MS inner binary that merged at different points after the merger time. The same as Figure 5 but also includes merged stars after they evolved to become WDs.

Appendix B
Companion Masses in BSS Binaries

The companions to BSSs can give insight into the formation history of the BSS. A. M. Geller & R. D. Mathieu (2011) found that the BSS binaries with periods around 1000 days have companion masses (M_2) that peak around $\sim 0.5\,M_\odot$. These masses were determined by fitting the mass function statistically. In Figure 8, we show the distribution for the companion masses for the simulated BSS binaries with similar periods from the triple-merger channel. We plot the M_2 distribution for our BSS binaries 10 Myr, 50 Myr, and 100 Myr after the merger event. Similar to A. M. Geller & R. D. Mathieu (2011), the M_2 distribution peaks around 0.4–0.8 $M_\odot$. As the binary evolves, the distribution becomes more localized in the aforementioned mass range.

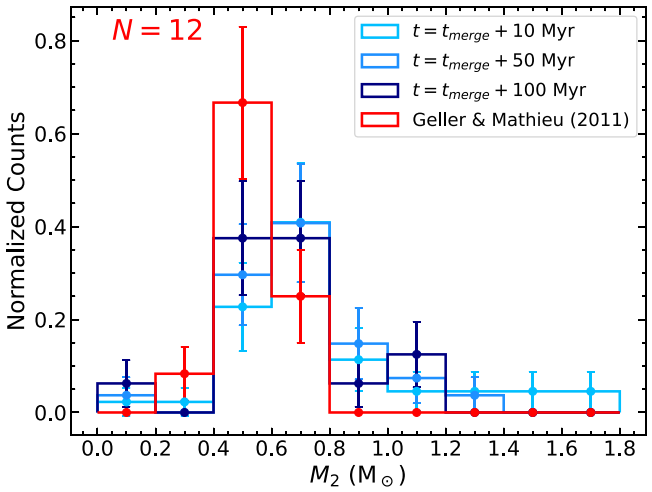

Figure 8. Masses of BSS binaries with orbital periods of the order of 1000 days. The red distribution represents the companion mass of 12 BSS binaries in NGC 188 with periods of the order of 1000 days. To compare with the observed distribution, we plot the companion for the simulated BSS binaries formed from the triple-merger channel. We only consider the simulated systems with $P_{orb} < 5000$ days at 10, 50, and 100 Myr after the merger.

ORCID iDs

Cheyanne Shariat https://orcid.org/0000-0003-1247-9349
Smadar Naoz https://orcid.org/0000-0002-9802-9279
Kareem El-Badry https://orcid.org/0000-0002-6871-1752
Antonio C. Rodriguez https://orcid.org/0000-0003-4189-9668
Bradley M. S. Hansen https://orcid.org/0000-0001-7840-3502
Isabel Angelo https://orcid.org/0000-0002-9751-2664
Alexander P. Stephan https://orcid.org/0000-0001-8220-0548

References

Adams, F. C., Ruden, S. P., & Shu, F. H. 1989, ApJ, 347, 959
Andrews, J. J., Taggart, K., & Foley, R. 2022, arXiv:2207.00680
Angelo, I., Naoz, S., Petigura, E., et al. 2022, AJ, 163, 227
Antonini, F., Chatterjee, S., Rodriguez, C. L., et al. 2016, ApJ, 816, 65
Antonini, F., Toonen, S., & Hamers, A. S. 2017, ApJ, 841, 77
Balaguer-Núñez, L., Galadí-Enríquez, D., & Jordi, C. 2007, A&A, 470, 585
Bate, M. R. 2012, MNRAS, 419, 3115
Bate, M. R., & Bonnell, I. A. 1997, MNRAS, 285, 33
Belloni, D., Schreiber, M. R., Zorotovic, M., et al. 2018, MNRAS, 478, 5626
Bergeron, P., Wesemael, F., & Beauchamp, A. 1995, PASP, 107, 1047
Bobrick, A., Davies, M. B., & Church, R. P. 2017, MNRAS, 467, 3556
Bode, M. F., & Evans, A. 2008, Classical Novae, 43 (Cambridge: Cambridge Univ. Press)
Bond, H. E., Henden, A., Levay, Z. G., et al. 2003, Natur, 422, 405
Breivik, K., Mingarelli, C. M. F., & Larson, S. L. 2020a, ApJ, 901, 4
Breivik, K., Coughlin, S., Zevin, M., et al. 2020b, ApJ, 898, 71
Busso, M., Gallino, R., & Wasserburg, G. J. 1999, ARA&A, 37, 239
Carney, B. W., Latham, D. W., Laird, J. B., Grant, C. E., & Morse, J. A. 2001, AJ, 122, 3419
Carney, B. W., Lee, J.-W., & Dodson, B. 2005, AJ, 129, 656
Chen, X., & Han, Z. 2008, MNRAS, 387, 1416
Cheng, S. J., Vinson, A. M., & Naoz, S. 2019, MNRAS, 489, 2298

Conroy, K. E., Prša, A., Stassun, K. G., et al. 2014, AJ, 147, 45
Cournoyer-Cloutier, C., Tran, A., Lewis, S., et al. 2021, MNRAS, 501, 4464
Dale, J. E., & Davies, M. B. 2006, MNRAS, 366, 1424
de Mink, S. E., Sana, H., Langer, N., Izzard, R. G., & Schneider, F. R. N. 2014, ApJ, 782, 7
Deheuvels, S., Ballot, J., Gehan, C., & Mosser, B. 2022, A&A, 659, A106
Donati, J. F., & Landstreet, J. D. 2009, ARA&A, 47, 333
Dorozsmai, A., Toonen, S., Vigna-Gomez, A., de Mink, S. E., & Kummer, F. 2024, MNRAS, 527, 9782
Duchêne, G., & Kraus, A. 2013, ARA&A, 51, 269
Dupuy, T. J., & Liu, M. C. 2011, ApJ, 733, 122
Duquennoy, A., & Mayor, M. 1991, A&A, 248, 485
Eggleton, P. P., Kiseleva, L. G., & Hut, P. 1998, ApJ, 499, 853
Eggleton, P. P., Kisseleva-Eggleton, L., & Dearborn, X. 2007, in IAU Symp. 240, Binary Stars as Critical Tools & Tests in Contemporary Astrophysics, ed. W. I. Hartkopf, P. Harmanec, & E. F. Guinan (Cambridge: Cambridge Univ. Press), 347
El-Badry, K., & Rix, H.-W. 2018, MNRAS, 480, 4884
El-Badry, K., Rix, H.-W., & Heintz, T. M. 2021, MNRAS, 506, 2269
El-Badry, K., Simon, J. D., Reggiani, H., et al. 2024a, OJAp, 7, 27
El-Badry, K., Rix, H.-W., Latham, D. W., et al. 2024b, OJAp, 7, 58
Escorza, A., Karinkuzhi, D., Jorissen, A., et al. 2019, A&A, 626, A128
Ferrario, L., Melatos, A., & Zrake, J. 2015, SSRv, 191, 77
Fields, C. E., Farmer, R., Petermann, I., Iliadis, C., & Timmes, F. X. 2016, ApJ, 823, 46
Fontaine, G., Brassard, P., & Bergeron, P. 2001, PASP, 113, 409
Fossati, L., Castro, N., Schöller, M., et al. 2015, A&A, 582, A45
Fregeau, J. M., Richer, H. B., Rasio, F. A., & Hurley, J. R. 2009, ApJL, 695, L20
Freitag, M., & Benz, W. 2005, MNRAS, 358, 1133
Gaia Collaboration, Prusti, T., de Bruijne, J. H. J., et al. 2016, A&A, 595, A1
Gao, Y., Toonen, S., & Leigh, N. 2023, MNRAS, 518, 526
Geller, A. M., Hurley, J. R., & Mathieu, R. D. 2013, AJ, 145, 8
Geller, A. M., Latham, D. W., & Mathieu, R. D. 2015, AJ, 150, 97
Geller, A. M., Leiner, E. M., Bellini, A., et al. 2017, ApJ, 840, 66
Geller, A. M., & Mathieu, R. D. 2011, Natur, 478, 356
Geller, A. M., & Mathieu, R. D. 2012, AJ, 144, 54
Geller, A. M., Mathieu, R. D., Harris, H. C., & McClure, R. D. 2009, AJ, 137, 3743
Geller, A. M., Mathieu, R. D., Latham, D. W., et al. 2021, AJ, 161, 190
Glebbeek, E., & Pols, O. R. 2008, A&A, 488, 1017
Goodman, A. A., Benson, P. J., Fuller, G. A., & Myers, P. C. 1993, ApJ, 406, 528
Gosnell, N. M., Leiner, E. M., Mathieu, R. D., et al. 2019, ApJ, 885, 45
Gosnell, N. M., Mathieu, R. D., Geller, A. M., et al. 2014, ApJL, 783, L8
Grishin, E., & Perets, H. B. 2022, MNRAS, 512, 4993
Hallakoun, N., Shahaf, S., Mazeh, T., Toonen, S., & Ben-Ami, S. 2023, ApJL, 970, L11
Hamers, A. S., Glanz, H., & Neunteufel, P. 2022, ApJS, 259, 25
Hamers, A. S., & Thompson, T. A. 2019, ApJ, 882, 24
Hansen, B. M. S., Kulkarni, S., & Wiktorowicz, S. 2006, AJ, 131, 1106
Hansen, T. T., Andersen, J., Nordström, B., et al. 2016, A&A, 588, A3
Heintz, T. M., Hermes, J. J., El-Badry, K., et al. 2022, ApJ, 934, 148
Heintz, T. M., Hermes, J. J., Tremblay, P. E., et al. 2024, ApJ, 969, 68
Hernandez, M. S., Schreiber, M. R., Parsons, S. G., et al. 2022, MNRAS, 517, 2867
Hinkle, K. H., Fekel, F. C., Joyce, R. R., et al. 2006, ApJ, 641, 479
Hinkle, K. H., Fekel, F. C., Joyce, R. R., et al. 2019, ApJ, 872, 43
Hinkle, K. H., Fekel, F. C., Straniero, O., et al. 2024, ApJ, 969, 35
Hurley, J. R., Pols, O. R., & Tout, C. A. 2000, MNRAS, 315, 543
Hurley, J. R., Tout, C. A., & Pols, O. R. 2002, MNRAS, 329, 897
Hut, P. 1980, A&A, 92, 167
Iben, I. J., & Renzini, A. 1983, ARA&A, 21, 271
Inutsuka, S.-I., & Miyama, S. M. 1992, ApJ, 388, 392
Ivanova, N., Heinke, C. O., Rasio, F. A., Belczynski, K., & Fregeau, J. M. 2008, MNRAS, 386, 553
Ivanova, N., Justham, S., Chen, X., et al. 2013, A&ARv, 21, 59
Jadhav, V. V., Pandey, S., Subramaniam, A., & Sagar, R. 2021, JApA, 42, 89
Jorissen, A., Boffin, H. M. J., Karinkuzhi, D., et al. 2019, A&A, 626, A127
Kaib, N. A., & Raymond, S. N. 2014, ApJ, 782, 60
Kippenhahn, R., Weigert, A., & Hofmeister, E. 1967, MComP, 7, 129
Kiseleva, L. G., Eggleton, P. P., & Mikkola, S. 1998, MNRAS, 300, 292
Knigge, C., Baraffe, I., & Patterson, J. 2011, ApJS, 194, 28
Knigge, C., Toonen, S., & Boekholt, T. C. N. 2022, MNRAS, 514, 1895
Kozai, Y. 1962, AJ, 67, 591
Kratter, K. M., Matzner, C. D., & Krumholz, M. R. 2008, ApJ, 681, 375
Kroupa, P., Tout, C. A., & Gilmore, G. 1993, MNRAS, 262, 545
Krumholz, M. R., Klein, R. I., McKee, C. F., Offner, S. S. R., & Cunningham, A. J. 2009, Sci, 323, 754
Kulkarni, S. R., Ofek, E. O., Rau, A., et al. 2007, Natur, 447, 458
Kummer, F., Toonen, S., & de Koter, A. 2023, A&A, 678, A60
Kuntz, A. 2022, PhRvD, 105, 024017
Lagos, F., Schreiber, M. R., Parsons, S. G., et al. 2022, MNRAS, 512, 2625
Larson, R. B. 1972, NPhS, 236, 7
Latham, D. W. 2007, HiA, 14, 444
Lauterborn, D. 1970, A&A, 7, 150
Lee, A. T., Offner, S. S. R., Kratter, K. M., Smullen, R. A., & Li, P. S. 2019, ApJ, 887, 232
Leigh, N., & Sills, A. 2011, MNRAS, 410, 2370
Leigh, N. W. C., & Geller, A. M. 2013, MNRAS, 432, 2474
Leiner, E., Mathieu, R. D., Vanderburg, A., Gosnell, N. M., & Smith, J. C. 2019, ApJ, 881, 47
Leonard, P. J. T. 1989, AJ, 98, 217
Li, Y., Bedding, T. R., Murphy, S. J., et al. 2022, NatAs, 6, 673
Lidov, M. L. 1962, P&SS, 9, 719
Liebert, J., Bergeron, P., & Holberg, J. B. 2005, ApJS, 156, 47
Lim, H., & Rodriguez, C. L. 2020, PhRvD, 102, 064033
Lombardi, J., Rasio, F., & Shapiro, S. 1995, ApJL, 445, L117
Lombardi, J. C. J., Rasio, F. A., & Shapiro, S. L. 1996, ApJ, 468, 797
Lombardi, J. C. J., Warren, J. S., Rasio, F. A., Sills, A., & Warren, A. R. 2002, ApJ, 568, 939
Lu, C. X., & Naoz, S. 2019, MNRAS, 484, 1506
MacLeod, M., Macias, P., Ramirez-Ruiz, E., et al. 2017, ApJ, 835, 282
Manchester, R. N., Hobbs, G. B., Teoh, A., & Hobbs, M. 2005, AJ, 129, 1993
Mardling, R. A., & Aarseth, S. J. 2001, MNRAS, 321, 398
Mathieu, R. D., & Geller, A. M. 2009, Natur, 462, 1032
Matsumoto, T., & Metzger, B. D. 2022, ApJ, 938, 5
Matteuzzi, M., Montalbán, J., Miglio, A., et al. 2023, A&A, 671, A53
McCrea, W. H. 1964, MNRAS, 128, 147
Metzger, B. D., & Pejcha, O. 2017, MNRAS, 471, 3200
Meyer, D. M.-A., Kuiper, R., Kley, W., Johnston, K. G., & Vorobyov, E. 2018, MNRAS, 473, 3615
Michaely, E. 2021, MNRAS, 500, 5543
Michaely, E., & Perets, H. B. 2014, ApJ, 794, 122
Michaely, E., & Perets, H. B. 2016, MNRAS, 458, 4188
Michaely, E., & Perets, H. B. 2019, ApJL, 887, L36
Michaely, E., & Perets, H. B. 2020, MNRAS, 498, 4924
Milone, A. P., Piotto, G., Bedin, L. R., et al. 2012, A&A, 540, A16
Moe, M., & Di Stefano, R. 2017, ApJS, 230, 15
Moeckel, N., & Bally, J. 2007, ApJL, 661, L183
Nagarajan, P., El-Badry, K., Lam, C., & Reggiani, H. 2024, PASP, 136, 074202
Naoz, S. 2016, ARA&A, 54, 441
Naoz, S., & Fabrycky, D. C. 2014, ApJ, 793, 137
Naoz, S., Fragos, T., Geller, A., Stephan, A. P., & Rasio, F. A. 2016, ApJL, 822, L24
Naoz, S., Kocsis, B., Loeb, A., & Yunes, N. 2013, ApJ, 773, 187
Nelemans, G., Portegies Zwart, S. F., Verbunt, F., & Yungelson, L. R. 2001, A&A, 368, 939
Nine, A. C., Mathieu, R. D., Gosnell, N. M., & Leiner, E. M. 2023, ApJ, 944, 145
Nine, A. C., Mathieu, R. D., Schuler, S. C., & Milliman, K. E. 2024, ApJ, 970, 187
Nine, A. C., Milliman, K. E., Mathieu, R. D., et al. 2020, AJ, 160, 169
Offner, S. S. R., Moe, M., Kratter, K. M., et al. 2023, in ASP Conf. Ser. 534, Protostars and Planets VII, ed. S. Inutsuka et al. (San Francisco, CA: ASP), 275
Ostriker, E. C. 1994, ApJ, 424, 292
Ostriker, E. C., Gammie, C. F., & Stone, J. M. 1999, ApJ, 513, 259
Paczyński, B. 1971, ARA&A, 9, 183
Pala, A. F., Gansicke, B. T., Townsley, D., et al. 2017, MNRAS, 466, 2855
Pandey, S., Subramaniam, A., & Jadhav, V. V. 2021, MNRAS, 507, 2373
Pejcha, O., Metzger, B. D., & Tomida, K. 2016, MNRAS, 455, 4351
Perets, H. B., & Fabrycky, D. C. 2009, ApJ, 697, 1048
Perets, H. B., & Kratter, K. M. 2012, ApJ, 760, 99
Preece, H. P., Hamers, A. S., Battich, T., & Rajamuthukumar, A. S. 2022, MNRAS, 517, 2111
Pribulla, T., & Rucinski, S. M. 2006, AJ, 131, 2986
Qureshi, A., Naoz, S., & Shkolnik, E. L. 2018, ApJ, 864, 65
Raghavan, D., McAlister, H. A., Henry, T. J., et al. 2010, ApJS, 190, 1
Rajamuthukumar, A. S., Hamers, A. S., Neunteufel, P., Pakmor, R., & de Mink, S. E. 2023, ApJ, 950, 9

Rappaport, S., Deck, K., Levine, A., et al. 2013, ApJ, 768, 33
Rose, S. C., Naoz, S., & Geller, A. M. 2019, MNRAS, 488, 2480
Rui, N. Z., & Fuller, J. 2021, MNRAS, 508, 1618
Rui, N. Z., & Fuller, J. 2024, OJAp, 7, 81
Sandage, A. R. 1953, AJ, 58, 61
Sarajedini, A., von Hippel, T., Kozhurina-Platais, V., & Demarque, P. 1999, AJ, 118, 2894
Schneider, F. R. N., Podsiadlowski, P., Langer, N., Castro, N., & Fossati, L. 2016, MNRAS, 457, 2355
Schreiber, M. R., Zorotovic, M., & Wijnen, T. P. G. 2016, MNRAS, 455, L16
Shahaf, S., Hallakoun, N., Mazeh, T., et al. 2024, MNRAS, 529, 3729
Shappee, B. J., & Thompson, T. A. 2013, ApJ, 766, 64
Shariat, C., Naoz, S., Hansen, B. M. S., et al. 2023, ApJL, 955, L14
Sills, A., Adams, T., & Davies, M. B. 2005, MNRAS, 358, 716
Sills, A., Adams, T., Davies, M. B., & Bate, M. R. 2002, MNRAS, 332, 49
Sills, A., Faber, J. A., Lombardi, J. C. J., Rasio, F. A., & Warren, A. R. 2001, ApJ, 548, 323
Sills, A., Karakas, A., & Lattanzio, J. 2009, ApJ, 692, 1411
Sills, A., Lombardi, J. C. J., Bailyn, C. D., et al. 1997, ApJ, 487, 290
Soker, N., & Tylenda, R. 2006, MNRAS, 373, 733
Starrfield, S., Iliadis, C., & Hix, W. R. 2016, PASP, 128, 051001
Stegmann, J., Antonini, F., & Moe, M. 2022, MNRAS, 516, 1406
Stephan, A. P., Naoz, S., & Gaudi, B. S. 2018, AJ, 156, 128
Stephan, A. P., Naoz, S., & Gaudi, B. S. 2021, ApJ, 922, 4
Stephan, A. P., Naoz, S., Gaudi, B. S., & Salas, J. M. 2020, ApJ, 889, 45
Stephan, A. P., Naoz, S., Ghez, A. M., et al. 2016, MNRAS, 460, 3494
Stephan, A. P., Naoz, S., & Zuckerman, B. 2017, ApJL, 844, L16
Stephan, A. P., Naoz, S., Ghez, A. M., et al. 2019, AAS/Division of Dynamical Astronomy Meeting, 51, 202.02
Strom, S. E., Strom, K. M., & Bregman, J. N. 1971, PASP, 83, 768
Sun, M., Mathieu, R. D., Leiner, E. M., & Townsend, R. H. D. 2021, ApJ, 908, 7
Temmink, K. D., Toonen, S., Zapartas, E., Justham, S., & Gänsicke, B. T. 2020, A&A, 636, A31
Tohline, J. E. 2002, ARA&A, 40, 349
Tokovinin, A. 2014a, AJ, 147, 87
Tokovinin, A. 2014b, AJ, 147, 86
Tokovinin, A. A. 1997, AstL, 23, 727
Toonen, S., Boekholt, T. C. N., & Portegies Zwart, S. 2022, A&A, 661, A61
Toonen, S., Hamers, A., & Portegies Zwart, S. 2016, ComAC, 3, 6
Toonen, S., & Nelemans, G. 2013, A&A, 557, A87
Toonen, S., Portegies Zwart, S., Hamers, A. S., & Bandopadhyay, D. 2020, A&A, 640, A16
Trani, A. A., Rastello, S., Di Carlo, U. N., et al. 2022, MNRAS, 511, 1362
Tremblay, P.-E., Cummings, J., Kalirai, J. S., et al. 2016, MNRAS, 461, 2100
Tylenda, R., & Soker, N. 2006, A&A, 451, 223
Tylenda, R., Hajduk, M., Kamiński, T., et al. 2011, A&A, 528, A114
Vaidya, K., Panthi, A., Agarwal, M., et al. 2022, MNRAS, 511, 2274
van Haaften, L. M., Nelemans, G., Voss, R., Wood, M. A., & Kuijpers, J. 2012, A&A, 537, A104
von Zeipel, H. 1910, AN, 183, 345
Yamaguchi, N., El-Badry, K., Ciardi, D. R., et al. 2024a, PASP, 136, 074201
Yamaguchi, N., El-Badry, K., Fuller, J., et al. 2024b, MNRAS, 527, 11719
Yungelson, L. R., Kuranov, A. G., & Postnov, K. A. 2019, MNRAS, 485, 851
Zenati, Y., Toonen, S., & Perets, H. B. 2019, MNRAS, 482, 1135
Zorotovic, M., Schreiber, M. R., García-Berro, E., et al. 2014, A&A, 568, A68